DEPOSITION OF TIN OXIDE FILMS BY SPRAY HYDROLYSIS AND CHARACTERISATION

A Thesis Submitted
in Partial Fulfilment of the Requirements
for the Degree of

MASTER OF TECHNOLOGY

By

B. R. SRIDHAR

to the

INTERDISCIPLINARY PROGRAMME IN MATERIALS SCIENCE

INDIAN INSTITUTE OF TECHNOLOGY KANPUR

AUGUST, 1980

CERTIFICATE

This is to certify that the thesis entitled "Deposition of Tin Oxide Films by Spray Hydrolysis and Characterisation" by B.R. Sridhar is a record of work carried out under my supervision and has not been submitted elsewhere for a degree.

Dr. S. Kar
Department of Electrical Engineering
and
Materials Science Programme,
Indian Institute of Technology, Kanpur

August 16, 1980.

Acknowledgement

I take this opportunity to express my most sincere thanks to Dr. S. Kar, who has done more than simply guiding me throughout the course of this work. The present effort has been the outcome of many a useful suggestion of Dr. Kar's and I consider it a previlege to have associated with him in this work.

I would thank Dr. T.R. Ramachandran for his most helpful hand in enlightening me about TEM analysis and Dr. K.N. Swamyrao, for his generous help in rendering the present work easier by providing some accessories needed.

I am also thankful to Mr. Ravi Sharma for his constant help throughout the fabrication work and to Mr. Rajan Varughese, S. Bhattacharya, S. Varma for their help and cooperation throughout the course of experimental work. I am indebted to Dr. K.S. Chari for his constructive criticisms and suggestions.

Finally thanks are also due for Mr. B.N. Srivastva for neat tracings and to Mr. L.S. Bajpai for excellent typing.

Notations

a_i	constant
A	active area of the cell, [cm^2]
c	velocity of light, [cm/sec];
	differential capacitance, [F]
d_{hkl}	interplanar spacing, [Å]
E_c	conduction band edge, [eV]
E_{FS}	Fermi level in Si, [eV]
E_v	valence band edge, [eV]
F	fill factor
h	Planck's constant, [erg.sec.];
	index of the plane
I	device current, [A];
	intensity of transmitted light, [mW/cm^2]
I_o	diode saturation current, [A];
	intensity of incident light, [mW/cm^2]
I_D	diode current, [A]
I_L	light generated current, [A]
J_L	light generated current density, [A/cm^2]
J_{SC}	short circuit current density, [A/cm^2]
J_{TT}	themionic tunneling current density, [A/cm^2]
k	index to the plane;
	Boltzmann's constant, [$eV/^oK$]
l	index to the plane;
	carrier mean free path, [cm]
m^*	effective mass of electron in conduction band, [g]

n	diode quality factor;
	carrier concentration, [cm^{-3}]
N	free electron concentration, [cm^{-3}]
N_c	effective density of states,
N_D	donor density, [cm^{-3}]
N_e	electron concentration, [cm^{-3}]
P_{IN}	power input on a solar cell, [mW/cm^2]
q	electronic charge, [C]
Q_{is}^{o}	interface state charge density at zero bias, [C/cm^2]
Q_{is}^{oc}	interface state charge density in open circuit condition, [C/cm^2]
R	series resistance of the cell, [Ohm]
R_s	sheet resistivity, [Ohms per square]
t	film thickness, [Å]
T	absolute temperature, [^{o}K]
T_T^{oc}	tunneling transmission factor in open circuit condition
V	device voltage, [V]
V_{oc}	open circuit voltage, [V]
V_{ox}	oxide voltage, [V]
V_{ox}^{oc}	oxide voltage in open circuit condition, [V]
ϕ_B^n	Schottky barrier height for n-Si, [V]
ϕ_n	$(E_c-E_{FS})/q$ for n-Si, [V]
ϕ_n^{TC}	figure of merit for transparent semiconductor, [Ohm^{-1}]
φ_i	interface potential, [V]
φ_i^{o}	interface potential at zero bias, [V]

φ_i^{oc}	interface potential at open circuit, [V]
ε_{ox}	oxide permittivity, [F/cm]
ε_s	silicon permittivity, [F/cm]
λ	wavelength of light, [Å]
$h\nu$	photon energy, [eV]
ν	frequency of light, [Ccps]
η	conversion efficiency of solar cell, [%]
χ_s	electron affinity in Si, [eV]
χ_{TC}	electron affinity in transparent conductor (SnO_2), [
δ	thickness oxide layer, [Å].

ABSTRACT

The aim of the present investigation was to deposit thin films of a transparent oxide semiconductor such as tin oxide and carry out characterisations with respect to its applications in solar cells. The chemical spray method adopted for depositing these films is quite simple and economical. The same method can be employed for depositing thin films of indium oxide and indium tin oxide (ITO), which are finding considerable applications in photovoltaics.

The deposited films have been found to possess good electrical and optical properties viz. resistivities of the order of 10^{-2} to 10^{-3} Ohm.cm and optical transmittances of the order of 80-90 percent. Heterojunction cells have also been made by depositing the film on single crystal n-Si. The electrical characterisation of the cells has been carried out. The analysis of the cells has yielded a conversion efficiency of 0.10 percent. The low efficiency of the cells has been attributed to the high series resistance arising from the large sheet resistivity of the tin oxide layer.

Modifications in the present method by way of changing over to fused silica in place of pyrex glass used in the present investigation as material for furnace tube, addition of dopants in suitable proportions to the spraying tin chloride solution to enhance the conductivity of resulting films, can bring about considerable improvements and lead to solar cells with good conversion efficiency.

1. INTRODUCTION

Oxides of some metals are being increasingly employed in photovoltaic and solar thermal methods of solar energy conversio Some of the important oxides that have been thus reported are indium oxide [1,2], tin oxide [3,4], indium tin oxide (ITO) [5-7 The conventional p-n junction solar cells used in photovoltaic conversion are not at present considered to be attractive in so far as large scale production is concerned. The main reason for this lies in the higher cost of production of these cells arising from material, processing, and fabrication techniques. The present day tendency is towards reducing the cost of production c the solar cells by using new materials which besides being less costly can simplify the fabrication technique. The search for such materials has eventually led to the development of transparent semiconducting and conducting materials, which when used in the form of thin films have been found to meet these requireme

1.1. Transparent Conducting Films

Good optical transparency and high electrical conductivity are properties which are quite contradictory to each other. Good optical transparency demands thinner films whose conductivities are quite low and high conductivity requires thicker films whose optical transparencies are quite low. In case of metals used as transparent conducting films, the high optical absorption limits the thickness of the films to values less than 100 Å [8]. Such films are being employed in MOS and Schottky barrier solar cells.

The metallic oxides mentioned above have been found to possess transparent conducting properties. J.C.C. Fan and F.J. Bachner [7] describe the preparation and properties of indium tin oxide films and have reported optical transmission of 80-90 percent with resistivities of $5\text{-}15 \times 10^{-4}$ Ohm.cm. N.S. Changs and J.R. Sites [9], J.B. Dubow, et al.[10] have fabricated ITO solar cells and report conversion efficiency of 10-12 percent.

The most important properties from the point of view of fabrication of solar cells are (i) high optical transparency (80-9 percent) and (ii) high electrical conductivity (10^2-10^4 mho/cm). All of the oxide semiconductors above have very high band gaps of the order of 3.5 eV. Hence the material acts as a transparent window in the visible range.

The high conductivities which these oxides possess are attributed to native defects arising out of stoichiometric deficiencies [11].

1.2. Methods of Deposition

In general, four methods of depositing these films have been reported :

(i) Evaporation of the metals and subsequent oxidation [12];

(ii)(a) Reactive sputtering of the concerned metals [13];

(b) Deposition from pressed oxide targets by ion beam [14] or RF sputtering [5-7];

(iii) Chemical vapor deposition [15];

(iv) Deposition by means of a chemical spray [16-19].

Best films with very good optical and electrical properties have been obtained by RF sputtering from metal oxide targets. However, the process needs an elaborate and expensive set up which is not economical. JCC Fan [14] has prepared ITO films at low deposition temperatures by ion beam sputtering with optical transparencies between 80 and 90 percent and resistivities of the order of 10^{-3} Ohm.cm. K.P. SreeHarsha, et al. [20] have fabricated solar cells by depositing ITO by ion beam sputtering and have obtained efficiencies of the order of 14 percent.

Chemical vapor deposition is being used for preparing single crystals of tin oxide since a long time. T. Muranoi et al. [15] have deposited tin oxide films by this method at deposition temperatures as low as 250 °C and have reported good optical and electrical properties for such films.

Deposition by means of a chemical spray is very simple and economical. A spray deposition method of obtaining tin oxide films with good optical and electrical properties suitable for solar cell fabrication is described in the following.

1.3. Chemical Spray Technique

Tom Feng, et al. [17] describe this technique in the fabrication of ITO and tin oxide cells. The technique essentially involves using a solution of a suitable chemical compound normally a chloride and forcing it through a jet by an inert gas such as N_2 or Ar on to substrates heated to temperatures of the order of 400-600 °C. The process involving the deposition of a film using the acqueous solution of a compound is known as 'spray hydrolysis'

In case of water solutions of tin chloride ($SnCl_4$, $5H_2O$), the reaction [15] may represented by:

$$SnCl_4 + 2H_2O \longrightarrow SnO_2 + 4HCl.$$

Tin oxide is formed on the substrates with HCl gas as one of the products of the reaction. H. Kostlin, et al. [16] have deposited ITO films by chemical spray using an alchoholic solution of the compound mixture of indium chloride and tin chloride.

The important parameters [8] controlling the deposition rate in any chemical spray are (i) concentration of the solution; (ii) inlet gas flow rate; (iii) temperature of deposition; (iv) geometry of the substrates with respect to the spraying jet.

Tom Feng, et al. [17] have reported a deposition rate of 1000 Å/min at their deposition conditions. A.L. Fahrenbruch et a [21] have investigated metal oxide/Si heterojunction cells. They have reported that for the same composition, the deposition rates differ at different temperatures leading to corresponding changes in the resistivities of the films. As the temperature increases, the deposition rate at a particular composition decreases resulting in increased resistivity of the deposited films.

1.4. Tin Oxide Solar Cells

Tin oxide on n-Si forms a good heterojunction solar cell. Such cells have been reported as low cost photovoltaic devices by K. Kajiyama et al. [3], H. Kato et al. [4], J.B. Dubow et al. [10]. The main reasons for this are that

(i) tin oxide can be deposited by an easy method such as spraying, which is quite economical,

(ii) tin oxide on Si forms an effective antireflection coating in addition to serving as a barrier layer. This property has been attributed to the refractive index (= 2) of SnO_2 layer which lies in between that of air and silicon. Hence the cost incurred towards an additional layer of antireflection coating is avoided. Besides this tin oxide acts as a transparent window in the visible range and hence the SnO_2/Si solar cells have a wide spectral response and large output current [22].

The reports of the SnO_2/Si heterojunction first came from Kajiyama and Furukawa [3], who deposited SnO_2 semiconducting layers, 1 micron thick, by chemical vapor deposition from $SnCl_2$, $2H_2O$ using oxygen as a carrier gas. Silver paste was used to provide ohmic contacts to the SnO_2 layer. The efficiency of this cell was about 0.10 percent. The low efficiency was attributed to the high series resistance of SnO_2 layer. Nishino and Hamakawa [12] investigated the electrical and optical properties of Si-SnO_2 heterojunctions. The tin oxide layer in this case was deposited by a two step process involving evaporation of tin and its subsequent oxidation in the furnace. The current-voltage characteristics of this SnO_2/Si diode indicated a good rectification. However, the efficiency of the cell has not been reported.

A good efficiency of about 10 percent has been reported by Anderson in a private report. Kato, et al. [4] have fabricated SnO_2/Si solar cells by the spray deposition technique using a

solution of $SnCl_4$, $5H_2O$ in concentrated hydrochloric acid and water mixture taken in the ratio 1:5. The same method has been employed by Arizumi et al. [22] in the fabrication of SnO_2/Si heterojunction diodes. They have reported better spectral response and quicker response times for these cells than for p-n junction cells. E.Y. Wang and R.N. Legee [23] have used hydrolysis of stannic chloride for depositing thin films of SnO_2 to fabricate heterojunction cells. The method adopted here is essentially a chemical vapor deposition involving $SnCl_4$, $5H_2O$ which is melted in a hot zone and carried by the gas onto substrates heated to about 800 ^oK in a furnace.

The SnO_2/GaAs (n-n) and SnO_2/Ge (n-n) heterojunction cells fabricated by them are reported to have efficiencies of 1.2 percent and 0.8 percent respectively. For (n-p) SnO_2/Ge they have not observed any photovoltaic effect with current-voltage relationship being linear in the low bias range investigated.

2. THEORETICAL BACKGROUND

2.1 Electrical Properties

2.1.1 Resistivity of thin films

In case of four point probe measurement, the resistivity, [24] of a material in the form of an infinitely thin slice resting on an insulating support, is given by:

$$\rho = 4.532\ [V/I]\ t, \qquad (2.1)$$

where V is the voltage applied across the inner probes, I the current through the outer probes, and t the thickness of the film. The sheet resistance, R_s, is given by :

$$R_s = \rho/t = 4.532\ [V/I]. \qquad (2.2)$$

The resistivity of the film depends upon the temperature of deposition. The films deposited at higher temperatures show far lesser resistivity than those deposited at lower temperatures. Spraying technique does not yield films of low resistivity at temperatures below 300 ^{o}C [15]. T. Muranoi et al. [15] attribute the decrease in film resistivity with increase in temperature to the increase in mobility resulting from the large grain size, which reduces scattering at grain boundaries.

Since the band gap of tin oxide is quite large, the intrinsic carriers are not a factor [25]. The high conductivities of these films have been attributed to the presence of native defects such as oxygen vacancies, which contribute donor levels to the material. M. Nagasawa and S. Shinoyo [26] have studied the heat treatment in vacuum of SnO_2 single crystals. The purpose of this heat treatment was to enhance oxygen vacancies or in other words to reduce the crystals. The properties of such crystals, which are quite similar to those of Sb doped crystals, are interpreted with the concept of degenerate semiconductor. The electrical properties of SnO_2 are isotropic [27] in spite of its anisotropic crystal structure. Assuming $\mu_H/\mu = 1$, where μ is the drift mobility and μ_H, the Hall mobility, the authors have found that Hall mobility

of reduced crystals does not vary with temperature and is lower than that for as grown crystals, for which mobility decreases with increase in temperature. This leads to the fact, that the conduction electrons in reduced crystals are degenerate in the temperature range investigated. The degenerate temperature T_d is given by :

$$T_d = 4.231 \times 10^{-11} (m/m^*) N_e^{2/3}, \qquad (2.3)$$

where N_e is the carrier density, m^* the effective mass of electron. Taking $m^* = 0.15$ m, $T_d = 300$ ^oK for reduced crystals. The authors report, that μ_H is independent of T upto 200 ^oK. For temperatures less than 200 ^oK, the Hall mobility decreases with decrease in temperature. This suggests carrier scattering due to ionised impurities. It has been found by the analysis of Marley and Dockerty [28] that high temperature annealing of SnO_2 produces a level 100-150 meV deep according to

$$E_d = [150 - 8.7 \times 10^{-5} N_d^{1/3}] \text{ meV}, \qquad (2.4)$$

where N_d is the donor concentration. This level is attributed to oxygen vacancies. S. Samson and C.G. Fonstad [25] have identified the two donor levels at 34 meV and 140 meV as due to the first and second ionised states of oxygen vacancy. Annealing in H_2 above 900 ^oC leads to the introduction of a new donor level at (50 $\pm$ 5) meV deep which is deeper than the first oxygen level. These suggest that rather than oxygen being drawn out by the hydrogen to leave vacancies, hydrogen diffuses and forms a new donor level. Samson et al. [25] give the general expression for

conductivity as :

$$\sigma = \sigma_o + \sum_i A_i \, P_{O_2}^{1/a_i} \quad , \qquad (2.5)$$

where σ_o is the conductivity due to impurities and A_i includes mass action constant, mobility, and electronic charge all of which are independent of the partial pressure of oxygen (P_{O_2}). The value of a_i is found to be 6 which is attributable to oxygen vacancy.

The variations of the conductivity of the tin oxide films have been studied by Aboalf et al. [29]. They attribute this variation to a combination of departure from stoichiometry and the incorporation of chlorine in the films. Chlorine is found to be present upto an extent of 1.2 % (w/O) in the sprayed films. When the temperature of deposition increases the chlorine content decreases along with the oxygen content leading to increased film conductivity. The chlorine concentration is found to be much lower for films deposited in H_2 ambient. The electrical conductivity and carrier concentration are found to be the same at room and liquid nitrogen temperature (-196 °C). This shows almost complete ionisation of impurity centres at -196 °C and is in agreement with an impurity level less than or equal to 0.02 eV below the conduction band edge of SnO_2. X-ray data have shown that chlorine is incorporated in tin oxide lattice either interstitially or substitutionally since no chlorine containing phases were detected. Substitutional or Interstitial incorporation should give rise to donor levels thus increasing

conductivity and carrier concentration in n-SnO_2 films.

SnO_2 has a rutile structure with its unit cell containing four oxygen and two tin atoms, and has a volume of 71.6 $\mathring{A}^3$. One atomic percent (a/o) of substitutional chlorine would give rise to a carrier concentration of 8×10^{20} electrons per cm^3. But the observed carrier concentrations are of the order of 1.5 to 1.2 x $10^{20}/cm^3$. This suggests that part of the chlorine incorporated is rendered electrically inactive by a probable interaction with oxygen vacancies.

2.2 Optical Properties

2.2.1 Film transmittance

On account of its high band gap, tin oxide has a good optical transmittance. The optical transmittance 'T' for a transparent conductor can be defined as:

$$T = I/I_o = \exp(-\alpha t), \qquad (2.6)$$

where I_o is the intensity of incident light; I, that of the transmitted light; α, the absorption coefficient of the material of the film and t, the film thickness.

From (2.6), $\ln (I_o/I) = \alpha t.$ (2.7)

Knowing the thickness of the material, its absorption coefficient can be calculated using equation (2.7).

For transparent conductors, a parameter often used to characterise is a quantity called figure of merit, ϕ_{Tc}, defined as:

$$\phi_{Tc} = T^{10}/R_s, \qquad (2.8)$$

where T is the transmittance and 'R_s' the sheet resistivity in Ohms per square.

In defining the above figure of merit, G. Haacke [30] argues that if the normal T/R ratios are used to define the figure of merit, such a definition may break down when distinguishing the transparent semiconducting films practically. It may so happen, that films with very low sheet resistivities having low transmittance values may have higher T/R ratios than

those having slightly higher sheet resistivity and transmittance, but whose transparent conductor properties are far superior. Hence the definition of the figure of merit in the above manner has arisen out of practical necessity.

From equation (2.8), $\phi_{Tc} = \exp(-10\ \alpha t)/R_s$. (2.9

The sheet resistivity $R_s = \rho/t = 1/\sigma t$.

This leads to $\phi_{Tc} = \sigma t \exp(-10\ \alpha t)$. (2.1

Assuming a given sheet resistivity, from (2.10) it is clear that $\phi_{Tc} \propto \exp(-10\ \alpha t)$,

$$\propto \exp[-10\ \alpha(1/R_s\sigma)],$$

$$\propto \exp[-\text{constant}(\alpha/\sigma)]. \quad (2.1$$

Equation (2.11) shows that α/σ is a basic materials parameter determining the figure of merit of a transparent conductor.

From classical theory,

$$\sigma/\alpha = \pi\ c\ n\ \nu^2\ \tau^2, \quad (2.1$$

where n is the carrier concentration,

ν is the frequency of light,

τ is the free carrier relaxation time,

and $\tau = 1/v$,

with l as the mean free path and v as the velocity of carriers.

Figure of merit is large for small α/σ or large σ/α corresponding to large mean free paths.

The high absorption of metals in the visible range demands very thin films of the order of 100 Å to achieve sufficient transparency. At such thicknesses, problems of agglomeration are severe. However this effect is negligible in transparent semiconductors which allow large film thicknesses and thus reduce the effects due to agglomeration.

2.2.2 Optical band gap and absorption

Tin oxide absorbs only in UV due to its high band gap. The estimation of the band gap of the material can be made by knowing its absorption coefficient. A relationship of the type, $\alpha^{1/2} = h\nu - E_G$ (2.13), is reported to correspond to indirect optical transition [15] of tin oxide. In the above relation ν is the frequency of light and E_G, the band gap. The plot of $\alpha^{1/2}$ versus $h\nu$ is found to yield a linear portion, whose extrapolation to zero absorption coefficient gives an intercept on the photon energy axis corresponding to the band gap of the material.

The absorption edge for tin oxide is found to lie at 3500 Å corresponding to a value of 3.5 eV for band gap. However the position of the absorption edge depends upon the carrier concentration and is found to shift to lower wavelengths with increase in carrier concentration. T. Arai [31] has given an explanation for this as follows : The high carrier concentration, which leads to a high degree of degeneracy of the semiconductor, leaves a part of the conduction band of tin oxide completely

filled with respect to the conduction band edge. As a result of this, the electrons have to be transfered over the top of the partially filled conduction band rather than over the top of conduction band edge during the electronic transition across the band gap. This needs higher photon energy and causes a shift in the absorption edge of tin oxide to lower wavelengths.

In the infrared range, the energy is insufficient to cause electronic transition across the band gap. In such cases, the electrons in the conduction band can absorb infrared photons to rise to higher levels within the band. This phenomenon is often called infrared reflectivity and the minimum wavelength at which this occurs shifts to lower values, as carrier concentration increases. The classical theory also supports this free carrier absorption, when it defines this plasma wavelength (λ_P) as :

$$\lambda_P = 2\pi C (4\pi N e^2/\varepsilon_M m^*)^{-1/2}, \qquad (2.14)$$

where ε_M is the dielectric constant of the material and m^*, the effective mass for carriers in conduction band and N, the carrier concentration.

2.3 Structural Characterisation

The results of thin film investigation are subject to a meaningful interpretation, if the samples have been fully characterised and their structure and composition are well known. Thin films can consist of more than one phase, if this

is thermodynamically favored. Identification of such phases, if any, is important, since they may have influence over the properties of the film.

2.3.1 Structural characterisation by X-rays

Analysis of the X-ray diffractogram, obtained by scanning the sample in a crystal X-ray diffractometer, is an important aspect of this process. The structure of tin oxide is tetragonal with the lattice constants [32] as follows :

$$a_o = 4.738 \text{ Å} \quad \text{and} \quad c_o = 3.188 \text{ Å}.$$

The unit cell of the structure contains two tin oxide molecules. For any particular diffraction peak at an angle θ, Bragg's law of X-ray diffraction is satisfied. Each one of the peaks corresponds to a reflection from a plane (hkl) corresponding to the interplanar spacing d_{hkl}. From Bragg's law,

$$2\, d_{hkl} \sin\theta = n\lambda,$$

where n is the order of diffraction,

and λ is the wavelength of incident X-rays.

Taking $n = 1$ for the first order,

$$d_{hkl} = \lambda/2 \sin\theta.$$

Since λ and θ are known, the interplanar spacing d_{hkl} can be calculated. For tetragonal tin oxide, the interplanar spacing d_{hkl} is related to the indices and lattice constants a_o and c_o by:

$$d_{hkl} = 1/[(h^2+k^2/a_o^2) + (l^2/c_o^2)]^{1/2} \qquad (2.15)$$

This leads to $h^2+k^2 + (a_o^2/c_o^2)l^2 = (a_o/d_{hkl})^2$.

Taking the above values of a_o and c_o,

$$h^2+k^2 + 2.2\,l^2 = (a_o/d_{hkl})^2. \qquad (2.16)$$

The calculated values of d_{hkl} are substituted in the above equation and the values of h,k,l are chosen so as to satisfy the above equation. These values give a set values for the indices of each diffraction peak.

2.3.2 Structural characterisation by transmission electron microscopy

The nature of the film and its microstructure are important in any characterisation. In transmission mode, the grains of the film can be observed and grain sizes determined. The diffraction pattern of the film can give an idea of the nature of the film namely whether the film is crystalline, polycrystalline or amorphous. Crystalline films are characterised by strong diffraction spots arranged in a fashion depending on the crystal structure. Polycrystalline films are characterised by sharp and continuous concentric rings. If the film has a specific orientation, the continuous rings split into arcs. The amorphous films are characterised by diffused ring pattern. The radii of the rings in a polycrystalline film are related to the inter-planar spacing by :

$$Rd_{hkl} = \lambda L , \qquad (2.17)$$

where R is the radius of any ring on the diffraction pattern and λL, the camera constant.

To evaluate the interplanar spacing, the camera constant is to be known. To determine the camera constant, a standard gold pattern, whose interplanar spacings are known is taken and the radii of the diffraction rings measured. Since the interplanar spacing for each ring is known from the standard data, the camera constant can be determined. After the camera constant is established, the radii of the ring pattern of the given film can be measured and the corresponding d_{hkl} evaluated. Knowing d_{hkl}, the indexing of the diffraction rings can be carried out in the usual way.

2.4 Theoretical Aspects of SnO_2/SiO_x/n-Si Solar Cells

Solar cell being a current generator, its equivalent circuit takes the form of a diode in parallel with a constant current source and a series resistance (Fig. 2.1). The current voltage characteristic of such a device is given by :

$$I = I_D - I_L = I_o [\exp q(V+IR)/kT-1] - I_L, \quad (2.18)$$

where I_D is the diode current; I_o, the saturation current; V, the voltage developed across the cell; R, the series resistance and I_L, the constant photogenerated current.

Important parameters of a solar cell are its open circuit voltage (V_{oc}), short circuit current density (J_{sc}), fill factor (F), and efficiency, (η).

$$\eta = (V_{oc} J_{sc} F/P_{in}) \times 100 \quad \text{percent}, \quad (2.19)$$

where

$$V_{oc} = kT/q [\ln(I_L/I_o) + 1], \quad (2.20)$$

$$I_{sc} = I_o [\exp (q R I_{sc}/kT) - 1] - I_L, \quad (2.21)$$

and

$$F = (\text{Maximum power obtainable})/V_{oc} I_{sc}. \quad (2.22)$$

Kajiyama and Furukawa [3] described the electrical characteristics on the basis of an energy band diagram, in which SnO_2 forms a Schottky barrier at the interface. However, a thin layer of oxide of silicon will form at the interface during processing and this oxide layer can strongly affect the device performance [33]. In devices, where this oxide layer is too thick, the electrons cannot tunnel through the layer and this results in

photocurrent suppression [34] through the recombination of light generated holes with electrons in Si.

In analysing tin oxide cells the theory of MIS devices is useful. Fonash [35], Shewchun, Singh and Green [36], and Card and Yang [37] have discussed this in detail. According to Fonash, the interfacial insulating layer can be used to improve open circuit voltage and the light generated carrier response by field shaping. Shewchun proposes that the mechanism of current conduction is tunneling through the interfacial layer. For insulator thickness of 10 Å, the cell is shown to exhibit Schottky behavior.

The case of ITO/oxide/n-Si diode, which is similar to SnO_2/SiO_x/n-Si diode has been discussed by Kar et al. [38]. The ITO/oxide/n-Si diode is considered to be similar to MOS diodes because the indium tin oxide is degenerate with a carrier concentration of $10^{21}/cm^3$. Accordingly the energy band diagram is given in Fig. 2.2 in which SnO_2 band is flat similar to that of metal and the barrier region is confined to n-Si.

If φ_i^{oc} is the Si band bending at open circuit voltage, V_{oc}, and ϕ_n^{TC}, the height of the Fermi level above the conduction band of SnO_2, then, the open circuit voltage is given by,

$$V_{oc} = (\chi_{TC} - \chi_s)/q - [(\phi_n + \phi_n^{TC}) + (\varphi_i^{oc} + V_{ox}^{oc})], \qquad (2.23)$$

where V_{ox}^{oc} is the oxide potential at open circuit voltage. φ_i^{oc} in equation (2.23) has been evaluated by Kar [39] on the basis, that the current mechanism is thermionic tunneling. In such cases, the thermionic tunneling current density is given by:

$$J_{TT}^{oc} = T_T^{oc} A T^2 \exp(-q \phi_B/kT) [\exp q(\varphi_i^o - \varphi_i^{oc}/kT)-1]. \quad (2.24)$$

Taking $\phi_B^n = \varphi_i^o + \phi_n$, and $J_{TT}^{oc} = J_L$, the light generated current density:

$$\varphi_i^{oc} = [kT/q \ln(AT^2/J_L)] + kT/q \ln T_T^{oc} - \phi_n. \quad (2.25)$$

In the above expression T_T^{oc} is the tunneling transmission factor depending on voltage.

If the Richardson constant A is assumed as

$$A = 120 \text{ A/cm}^2/^oK^2, \quad T = 300 \ ^oK, \ J_L = 40 \text{ mA/cm}^2,$$

$$\varphi_i^{oc} = 0.50 \text{ V} + kT/q(\ln T_T^{oc}) - \phi_n. \quad (2.26)$$

Substituting equation (2.26) in (2.23) the expression for open circuit voltage reduces to:

$$V_{oc} = \varphi_i^o + \phi_n - [(kT/q) \ln T_T^{oc}] - 0.50 \text{ V} + (V_{ox}^o - V_{ox}^{oc}).$$

..... (2.27)

$$V_{ox}^o - V_{ox}^{oc} = (Q_{is}^o + Q_{is}^{oc}) t_{ox}/\varepsilon_{ox}, \quad (2.28)$$

where Q_{is}^o and Q_{is}^{oc} are interface charge densities at short circuit current and open circuit voltage respectively.

3. EXPERIMENTAL

3.1 Experimental Set-up

The set-up used for spraying tin chloride solution can be divided into three sections such as :

(i) sprayer unit,

(ii) furnace system, and

(iii) exhaust unit.

3.1.1 Sprayer unit

The unit is made of pyrex glass and is as shown in Fig. 3.1a. It is a selfcontained unit consisting of a reservoir 1 to hold the solution. The inlet gas enters through 2 and is allowed to expand in the bulb 5 before it issues out of the tapered end. The bulb can be exposed to atmosphere to stop the spray by means of stopcock 3. The solution suction tube 4 ends into a nozzle at the tapered end of the bulb 5. The entire unit consisting of reservoir and sprayer is attached to the ground glass socket 6 so as to facilitate the sprayer unit to be fixed to the cone of the furnace tube.

3.1.2 Furnace system

The furnace tube is of pyrex glass about two inches in diameter and one meter in length with two B-55 ground glass cones fitted at its ends. The tube is inserted into a furnace about three kilowatt capacity. The furnace is mounted on a rigid frame provided with castor wheels. The instrumentation needed for this

is mounted on a front panel made of 1/8" thick Al sheet. The instrumentation includes :

(i) a temperature controller, 3kW, associated with the furnace,

(ii) a Variac (230V, 15A),

(iii) an AC Ammeter (0-25 A), and

(iv) a switch socket combination for the input.

The temperature controller acts via a relay and a contactor to make the furnace on and off, whose period can be controlled by a potentiometer included in the system. The temperature of the furnace is read by a temperature indicator suitable for Chromel-Alumel thermocouple and is mounted on the front panel of the controller.

The current through the furnace is limited by the Variac included at the controller output with an ammeter in series. The ammeter is protected from being damaged when the controller is tripping on and off by bypass switches which connect the furnace directly to the controller output.

3.1.3 Exhaust unit

This consists of a B-55 ground glass socket to which is attached a glass tube through which a push rod and boat arrangement slides as shown in Fig. 3.1b. The push rod is actually a hollow tube (6 mm in diameter), about 75 cm in length, to the end of which a boat made of pyrex glass is attached. A Chromel-Alumel thermocouple passes through this tube to record the

temperature in the proximity of the boat.

The entire assembly inclusive of sprayer unit, furnace tube, and the exhaust unit is shown in Fig. 3.1b.

3.1.4 Experimental proceedure

To start with, the solution of a known concentration in deionised water is made. The sprayer unit is cleaned first by degreasing with TCE and removing traces of TCE by acetone. It is fixed into the furnace tube after applying vacuum grease to ground glass joints. At the exhaust end, the substrates on which deposition is to be carried out are loaded on to the boat and the exhaust unit is fitted to the furnace after applying vacuum grease around ground glass joints. The solution is poured into the reservoir of the sprayer unit.

The furnace is heated by passing about 14 A current adjusted through the Variac. The furnace is allowed to get heated continously by setting the potentiometer at 100 (for full heating). When the temperature closer to the deposition temperature is reached, the potentiometer setting is brought down to lower values such as 50 or 60 so that furnace trips on and off with the ammeter bypassed by the switches provided. A steady temperature (400 ^{o}C) is reached after sometime when the heating and cooling rates are equalised.

The inlet of the spraying unit is connected to a N_2 or Ar cylinder through a flowmeter. The pressure of the inlet gas is adjusted to be above the minimum required to start the spray. This minimum is to be noted previously by a separate trial

experiment. The gas flow rate is adjusted by opening the stopcock of the sprayer unit. When sufficient flow rate is established and the stopcock is closed, the spraying starts. The spraying is continued for known interval of time and then stopped by opening the stopcock. The HCl gas produced during the reaction is swept out by the inlet gas through the outlet tube connected to the exhaust.

In case any annealing in an inert ambient is required, the inlet gas pressure can be considerably reduced below the minimum required for the spray and then samples can be allowed to get heated at the deposition temperature or any temperature for known time intervals. The samples can be unloaded when the furnace cools off slightly.

3.2 Electrical Characterisation

3.2.1 Conductivity type

The deposited film was subjected to a test in which a hot probe was pressed on some point on the film and cold probe on some other point. The direction of deflection of the spot of light on the graduated scale of Leads and Northrup galvanometer was noted. The direction of deflection indicated the conductivity type of the deposited film.

3.2.2 Resistivity measurement

A four point probe was used for measuring the resistivity of the deposited film. The circuit arrangement for this consisted

of a power supply connected across the outer probes in series with an ammeter. The voltage across the inner probes was measured by a differential AC-DC Voltmeter Model 803B, John Fluke Manufacturing Co.

To start with, the voltmeter was adjusted for null deflection by placing the meter in the position 'Calibrate' and adjusting the pointer to read zero. The probes were pressed against the sample so that all the four probes made good contact with it. Current was increased in steps of 1 mA by adjusting the voltage from the power supply. In each case the voltmeter was balanced for null deflection by turning the knobs provided for this purpose and the voltage was read off directly corresponding to the position of the knobs.

Voltage versus current was plotted and the slope of the straight line determined the ratio V/I. The sheet resistivity of the film, R_s [Ohms per square] was calculated using the formula,

$$R_s = \rho/t = 4.532\ (V/I), \qquad (3.1)$$

where 'ρ' is the resistivity of the film and 't', the thickness. By knowing the thickness, the resistivity was calculated using the formula

$$\rho = R_s t. \qquad (3.2)$$

3.3 Optical Characterisation

3.3.1 Measurement of film thickness

A sharp step was obtained by covering a portion of the

substrate (glass) by another glass slide having a sharp edge. A uniform coating of Al about 1000 Å thick was obtained by evaporating Al from Grainville Philips Co, USA Vacuum coating unit. The thickness of the film was obtained by measuring the height of the step using an Angstromscope Interferometer.

Light from sodium vapor lamp is incident on a semireflecting plate called Fizeu plate after passing through semireflecting glass plates. The Fizeu plate can be tilted to a convenient position so as to form a wedge with the given sample. The straight dark and bright fringes can be seen through an eyepiece provided with a micrometer.

If the surface of the film is not uniform, this is reflected as an offset in the fringe system. Hence in the region between the film and the glass plate where there is a step, an offset in fringes is observed. By measuring the offset of fringes and the fringe spacing, the thickness of the film can be calculated using the formula,

$$t = (\text{offset/spacing}) \times 2946\ (\text{Å}). \qquad (3.3)$$

In these measurements, the offset and fringe spacing are expressed in filar units.

3.3.2 Transmittance measurements

3.3.2.1 Transmittance measurement using solar cell

A standard OCLI solar cell was used to measure the transmittance of films. The solar cell is mounted on a rigid metallic plate which also serves as a lead to the back contact

of the cell. The cell is surrounded by opaque metallic side covers with a rectangular opening on the top. An aluminium mask with a circular opening was so kept as to cover the entire opening other than the solar cell. This precaution was taken to avoid extraneous light from passing through the opening from its sides.

A bare glass slide similar to the one used as a substrate in tin oxide deposition was placed over the circular opening and a tungsten filament lamp was used to illuminate the cell area. The photocurrent was measured by using the VTVM in current mode and set to a convenient value by adjusting the position of the lamp. The glass slide on which the film was deposited was placed over the opening and the value of current read on the VTVM. The percent transmission was directly determined by considering the photocurrent with the bare glass slide as one hundred percent transmission.

3.3.2.2 Spectrophotometric measurements (normal incidence)

These measurements were carried out using a Toshnival type RL02 spectrophotometer employing a photomultiplier for wavelengths below 6000 Å and a red sensitive photocell above this wavelength. The set-up could be used to measure the transmittance accurately over a wavelength range of 3600 to 9000 Å.

The glass slide with the film was held in a sample holder. A bare glass slide was used as a reference standard in all these measurements and was held in a similar sample holder. Light source was a tungsten lamp. Appropriate wavelengths were selected

with the help of a quartz prism monochromator and the chosen beam was collimated first on to the clear glass slide to obtain the reference intensity and then on to film areas about 1 cm x 0.1 cm. By balancing the bridge circuit, the transmittance was read off directly from a calibrated dial. The use of reference slide enables the film transmittance to be obtained directly.

Care was taken to see that the sample was held such that the beam was incident at the air-film interface.

The values of transmittance were plotted against the corresponding wavelengths to determine the spectral characteristics of the deposited films.

The films on fused silica were separately scanned by the same method in Carey 17-D Ultraviolet-Visible Spectrophotometer and the transmittance versus wavelength and absorbance versus wavelength plots were recorded in the range of wavelength 2000 Å-7000 Å. From the plot of absorbance (A) versus wavelength, the absorption coefficients (α) of the film for various wavelengths were obtained using the formula,

$$\alpha = [2.3 \log (I_o/I)]/t = 2.3 [A/t], \qquad (3.4)$$

where A is the absorbance given by $A = \log [I_o/I]$, having I_o as the incident intensity and I as the transmitted intensity.

The square root of absorption coefficient versus the photon energy was plotted and the intercept on the photon energy ($h\nu$) axis of the extrapolated linear portion of the curve for zero absorption coefficient was obtained.

3.4 Studies on Thin Film Structure

3.4.1 X-ray characterisation

The deposited films were mounted on an X-ray crystal diffractometer. The samples were scanned by using copper K_{alpha} and iron K_{alpha} radiations in the range from 0^{o} to 100^{o}. The data obtained were traced by a recorder which moves in resonance with the rotation of X-ray diffractometer. The movement of the chart on the recorder was kept at 2^{o} per minute and the intensity was kept in the range of 1000 Cps. This experiment was carried out for different films and a record of the X-ray diffraction pattern (Intensity vs. 2θ) was obtained.

3.4.2 Transmission electron microscopic characterisation

Tin oxide is not attacked by most of the strong acids and bases. The samples for the TEM analysis were prepared by loosening the portions of the film deposited on glass by dipping in dilute hydrofluoric acid and floating them off in deionised water. The floating films were carefully picked by the copper grids. In this way the samples were prepared for films of different thickness.

The copper grids were placed in the path of an electron beam from an electron gun at 100 kV of a transmission electron microscope. The samples were seen in both transmission and diffraction modes and photographed.

3.5 Fabrication of Solar Cells

The solar cell fabrication includes the following steps : wafer cleaning, deposition of tin oxide layer, vacuum evaporation

of the back ohmic contact, vacuum evaporation of front contact. This sequence is clearly shown in Fig. 3.2.

3.5.1 Surface cleaning

Single crystal silicon (111) wafer about 250 micron thick and resistivity of 0.2 to 7.0 Ohm.cm obtained from General Diode Corporation, USA was the starting material. These had their front surface polished and back surface lapped. Chemical cleaning included treating with organic solvents and etching in HF. Prior to chemical cleaning, the wafers were cleaned ultrasonically. The sequence of steps was as follows.

(i) The wafer was degreased by treating in warm trichloroethylene for about 2 minutes, then in warm acetone for two minutes to remove traces of trichloroethylene, and finally in warm methanol for two minutes to remove traces of acetone.

(ii) The wafer was etched in dilute HF to remove the intrinsic oxide.

(iii) The wafer was decanted in deionised water several times to remove traces of HF.

(iv) The wafer was treated with warm HNO_3 for five minutes to grow a fresh layer of oxide about 50-60 Å thick.

(v) The wafer was decanted in deionised water several times to remove traces of acid.

(vi) The wafer was etched in HF to remove the freshly grown oxide.

(vii) The wafer was finally decanted in deionised water.

After this surface treatment proceedure, the polished surface of the wafer came out hydrophobic, which is a good indication of cleanliness. The presence of beads of water on a freshly etched wafer would indicate presence of contamination. Steps (iii) and (v) are necessary to avoid chemical etching of silicon, which in turn will affect the flatness of the surface. By removing the oxide grown in steps (iv) any mechanical damage and surface contamination are removed.

Surface cleaning of wafer is very critical in the fabrication of devices. Hence a clean chemical bench and electronic grade chemicals were used.

3.5.2 Tin oxide deposition

When the temperature of the furnace was about 300 ^{o}C, the wafers were loaded on the boat at the exhaust end of the furnace tube. Along with the wafer a clean glass slide partially covered by another thin microscopic slide was kept so that this could act as a representative sample of the film deposited on the wafer.

When a steady temperature of 400 ^{o}C had reached, the spraying was started, continued for 1.5 minutes and then stopped. The wafers were annealed at 400 ^{o}C in Ar ambient for about 25 minutes by reducing the inlet gas pressure below that needed for spray.

The samples were unloaded. The edges of the Si wafer were scribed to remove tin oxide deposited on the edges so as to

avoid conducting paths.

The thickness of the deposited layer was measured by using Angstromscope Interferometer and the resistivity, by the four point probe method. The sample deposited on glass was used in these measurements. The transmittance of the sample was measured by using a standard solar cell.

3.5.3 Metallisation

The metal (Al) evaporation was carried out in a high vacuum system (Grainville Philips Co., USA) equipped with a Perkin Elmer, USA, Model 605-1210 digital quartz thickness monitor. Any oil contamination of the chamber was minimised by the use of liquid nitrogen traps.

Helical coil tungsten filament was used for the evaporation of Al. The filaments were thoroughly degreased in warm trichloroethylene, acetone, and methanol and fired in vacuum for outgassing. The Al metal evaporated was obtained in 5 N purity in wire form. The metal was also degreased in the same way before use. Degassing of metal was done before each evaporation. While degassing a shutter was kept in between the source and the substrate to prevent any foreign volatile species from getting deposited on the substrate surface. Back ohmic contact of 1000 Å was deposited first and then the front contact through a mask with a circular opening of 2 millimeter diameter.

3.6 Measurements on Solar Cells

3.6.1 Current-voltage characteristics

The circuit diagram used for measuring dark current-voltage characteristics is shown in Fig. 3.4b. The tin oxide cell was placed over a copper block through which water could be circulated. The block itself acts as one of the contacts to the solar cell. The contact to the front surface was made by using a palladium-tipped spring probe. The tin oxide diode is forward biased when tin oxide is positive and silicon, negative. The forward I_D-V characteristic was obtained by increasing the voltage applied across the cell in steps and noting the corresponding current. During the measurements care was taken to see that no extraneous light affected the dark I-V by placing the cell in a light tight box. A similar experiment was carried out by making the tin oxide negative with respect to silicon so as to bias the diode in the reverse direction.

The semilogarthmic plots of current versus voltage were made. From the forward current-voltage characteristic, the diode ideality factor, 'n' was calculated at different points of the curve by using the formula,

$$n = q/kT(d \text{ In } I_D/dV). \qquad (3.5)$$

The series resistance of the cell was determined by plotting the forward currents vs. voltage on a linear graph and finding the slope of the curve in the linear region.

AM1 illumination was simulated with the help of a 150 W tungsten lamp and checked with the help of a commercial OCLI p-n junction solar cell. The current-voltage characteristic of the solar cell was measured as indicated in Fig. 3.4a. From the I-V characteristics of the solar cell, one could obtain the open circuit voltage, the short circuit current, and the fill factor. The efficiency of the cell was obtained by finding the maximum area of a rectangle that could be fitted into solar I-V characteristics. During the entire measurement of solar I-V, care was taken to see that the temperature of the device is kept constant by circulating water in the copper block.

3.6.2 Capacitance-voltage measurements

The C-V measurement on the cell was made in the dark at 100 kHz using the set-up shown in Fig. 3.4c. The a.c. signal voltage was measured with an a.c. voltmeter and kept below 15 mV. Complete shielding of the device was essential in dark C-V measurements as it had been observed that room light has a considerable effect on the capacitance of the cell. The device capacitance was measured upto considerably large reverse bias values. The reciprocal of the squared capacitance was plotted as a function of the bias and was found to be a straight line. From the slope of the line the doping density was found by knowing the area of the cell using the formula:

$$N_{doping} = 2/qA^2\varepsilon_s \left[d(1/C^2)/dV\right]. \qquad (3.6)$$

From the intercept of the straight line with the bias axis, the zero bias silicon band bending was obtained as given by:

$$\varphi_i^o = -V_{intercept} + kT/q. \tag{3.7}$$

The zero-bias barrier height on n-Si is given as:

$$\phi_B^n = \varphi_i^o + \phi_n, \tag{3.8}$$

where

$$\phi_n = [kT/q]\,[\ln N_c/N_D], \tag{3.9}$$

having N_c as the effective density of states and N_D as the doping density in Si.

4. RESULTS AND DISCUSSION

4.1 Electrical Characterisation

The conductivity type of all the deposited samples was found to be strongly n-type.

Table 4.1 indicates the sheet resistivities of the films obtained under different deposition conditions and times of spray. The deposition was made at 400 ^{o}C in some cases and 425 ^{o}C in some other cases. As can be seen from this table the sheet resistivity of the film is a function of thickness or deposition time. As the duration of spraying is increased, the thickness of the film increases and the sheet resistivity diminishes. In some cases, where the spray was not continuous as indicated in the remarks column on account of a pressure build-up in the furnace tube, which resulted in forcing the solution back to the reservoir, the thicknesses of the film are low and the corresponding sheet resistivities are higher. This can be seen in case of deposition numbers 3 and 12 where the sheet resistivities are far higher through their deposition times are comparable to those in other depositions. The sheet resistivities of films deposited on fused silica are lower than those of films deposited on glass as can be seen from deposition number 22. This can be attributed to the absence of alkali ions in fused silica substrate. Alkali ions are present in glass and are extremely mobile. As a result, they can easily diffuse into the deposited film and act as acceptors or capturing centres for electrons in addition to being an impurity

atom causing scattering in the tin oxide. The consequence of this is that the films deposited on glass are more resistive than those deposited on fused silica.

The resistivities of the deposited film are in the range of 10^{-2} to 10^{-3} Ohm.cm in all cases listed. The reproducibility of the properties of the film to a certain extent could be obtained in the last three depositions. In these depositions, the pressure of the inlet gas (Ar) could be fixed exactly at the needed value (12 psi) by using better gas regulator valves. Deposition numbers 21, 22, 23 reflect this. The spray was made continuous in all these depositions by slightly loosening the sprayer end, so that this is communicated to the atmosphere so as to reduce the pressure build-up in the furnace tube. The deposition indicates approximately a linear growth rate of 6000 Å/ minute and the sheet resistivity displays a gradual decrease with increase of deposition times. In depositions 18 and 20, two different films of the same deposition are showing different sheet resistivities. The reason for this lies in the fact that one of the substrates was found to have shifted from the main stream of the spraying jet. This resulted in different amounts of deposition - substrate directly in the line of spray receiving more deposition than the other. The different thicknesses arising out of this led to different sheet resistivities of the films.

4.2 Optical Characterisation

Table 4.1 shows also the optical transmittance of films

of different sheet resistivities. Figure 4.1 shows the variation of optical transmittance with sheet resistivity for films deposit on glass. Figure 4.1 indicates a certain trend, in which for sheet resistivities above about 70 Ohms per square, the film transmittance lies around or above 80 percent, where as those bel this show reduced optical transmittance of about 70 percent. However, for films deposited on fused silica the transmittance remains quite high (90 percent) even at sheet resistivities of the order of 63 Ohms per square, at which the film on glass shows a poor optical transmittance. Figure 4.2 shows the transmittance characteristics of films deposited on fused silica. The transmission remains between 70 and 80 percent in the visible range (4000 Å - 7000 Å). Figure 4.3 compares the transmittance characteristics of film deposited on fused silica with that deposited on glass. Once again the same trend, in which the film on fused silica, though thicker than that on glass, shows a better transmittance characteristics, is seen. One of the reasons for this is that the absorption of fused silica (SiO_2) is lower than that of glass and hence the corresponding transmittance is high. Owing to their high index of refraction the main losses in the optical transmission of the films on glass are caused by interference effects and by increases in the intensity of luminous reflection. Figure 4.4 shows the transmittance, reflectance, and absorptance characteristics of a film of sheet resistivity 180 Ohms per square deposited on glass. As can be seen from Fig. 4.4, the decrease of optical transmittance is marked by an increase in reflection and absorption. A maximum reflection of 20 percent at 4000 Å and

a minimum of about 5 percent are observed. Figure 4.5 shows the transmittance characteristics of films of different thicknesses and sheet resistivities. It can be readily seen that as the films become less and less resistive, the transmission characteristics become gradually poorer. One of the reasons for this is the increase of thickness as the films become less and less resistive, which is accompanied by an increase in optical absorption. Another reason advanced for poor transmission characteristics of films is the presence of SnO as a second phase in tin oxide (SnO_2) [29,31]. Since the band gap of SnO is smaller than that of SnO_2, the optical transmission diminishes.

Figure 4.6 shows a plot of square root of absorption coefficient vs photon energy (h). The extrapolation of the linear part to zero absorption coeffieient yields an intercept of 3.45 eV. This value is closer to the reported value, 3.42 eV, which is supposed to be due to indirect transition in tin oxide.

4.3 Structural Characterisation

4.3.1 X-ray analysis

Figure 4.7a is the X-ray diffractogram of tin oxide deposited on glass obtained by using iron K_{alpha} radiation. The strong diffraction peaks are indicative of polycrystalline nature of the film. The peaks of X-ray diffractogram are indexed as shown in Table 4.2. The underlined indices match with those given in the standard X-ray data (Table 4.3).

4.3.2 TEM analysis

Figure 4.7b gives the transmission electron diffraction pattern of tin oxide films. The diffraction pattern displays continuous rings indicating that the material is polycrystalline having a random orientation. The prominent rings have been indexed as given in Table 4.4.

Figures 4.8 and 4.9 indicate the transmission electron microscopic pattern of films of two resistivities. Figure 4.8 is the microstructure of the film deposited at 400 ^{o}C. The film has a sheet resistivity of about 4500 Ohms per square and a thickness of about 600 Å. As can be seen the film is interspersed with voids, which inhibit electrical conductivity and lead to large sheet resistivities as is the case. Figure 4.9 shows the microstructure of the film with a sheet resistivity of 123 Ohms per square. The film is about 4000 Å thick and can be seen to be almost continous. The same study indicated that the film is interspersed with black regions. However the identification of these regions could not be made since their diffraction patterns could not be recorded due to poor intensities.

4.4 Analysis of Tin Oxide Cells

Figure 4.10 shows the current-voltage characteristics of the tin oxide cell under AM1 illumination. From Fig. 4.10, it is found that the open circuit voltage of the cell is 275 mV and the short circuit current 340 microamperes. The active area of the cell was 20.9 mm^2. This yielded short circuit density of 1.6 mA/

The fill factor determined by finding the largest area of the rectangle that can be inserted in the current-voltage characteristics gave a value of 22 percent. The conversion efficiency of the cell was about 0.10 percent. Such low fill factor and short circuit current density may be attributed to the high series resistance arising from SnO_2 layer. The series resistance as determined from the linear portion of diode current-voltage characteristics as shown in Fig. 4.11 comes out to be 440 Ohms [90 $Ohm.cm^2$], which is rather quite large for a solar cell.

Figure 4.12 is a semilogarthmic plot of dark diode current (I_D) vs. voltage. From the forward characteristic the diode ideality factor (n) has been evaluated and found to be 2.5 and 4.7 at the two points indicated.

Figure 4.13 is a plot of reciprocal of squared capacitance versus voltage. The plot is a straight line. The extrapolation to zero value of reciprocal of squared capacitance yields for the zero bias silicon band bending (φ_i^o) a value of 0.75 V. The silicon doping density calculated by finding the slope of the straight line yields a value of $1.16 \times 10^{15}/cm^3$. The total barrier height turns out to be 1.0 V.

Table 4.1

Deposition Number	Substrate	Deposition time (secs.)	Deposition temp. (°C)	Film thickness (Å)	Transmittance (%)	Sheet resistivity Ohms per square	Resistivity Ohm. cm.	Figure of merit $(Ohm)^{-1} \times 10^{-3}$	Remarks
2	Glass	60	425	3900	83	125	4.77×10^{-3}	1.23	
3	Glass	120	425	2700	90	793	2.14×10^{-2}	0.44	Spraying discontinuous
4	Glass	180	420		89	145		2.15	
10	Glass	120	400	3000	86	476	2.81×10^{-2}	0.47	
11	Glass	160	400	3700	83	79	2.93×10^{-3}	1.96	
12	Glass	60	400		93	1845		0.26	Spray discontinuous, Annealing at 400 °C in N_2 for 15 minutes.
13	Glass	120	400	10,000	72	45	4.5×10^{-3}	0.83	Sample annealed at 400 °C in N_2 for 15 minutes.
17	Glass	60	400	4000	78	135	5.40×10^{-3}	0.79	Annealing in Ar for 10 minutes.
18	(a)Glass	90	400	3600	88	193	6.95×10^{-3}	1.44	Annealing in Ar for 15 minutes
	(b)Glass	90	400	4000	78	72	2.88×10^{-3}	1.16	
19	Fused Silica	45	400	2100	88	151	3.17×10^{-3}	1.84	Spray discontinuous, annealing at 400 °C for 15 minutes.

Table 4.1 (Continued)

20	Glass	(a)	45	400	4000	84	199	7.90×10^{-3}	0.88	Annealing in Ar for 15
		(b)	45	400	4400	80	123	5.40×10^{-3}	0.87	minutes.
21	Glass		30	400	2100	84	269	5.64×10^{-3}	0.65	Annealing in Ar for 15 minutes.
22	(a)Glass		45	400	4400	80	70	3.10×10^{-3}	1.53	Annealing in Ar for 15 minutes.
	(b)Fused silica		45	400	4500	90	63	2.83×10^{-3}	5.53	Annealing in Ar for 15 minutes.
23	Glass		90	400	9000	84	69	6.20×10^{-3}	2.53	Annealing in Ar for 25 minutes.

Deposition 2, 3, 4 were done at inlet gas pressure of 9 psi, 10 and 11, at 10 psi and 12 [illegible] at 12 psi, above the atmospheric pressure.

Table 4.1 (Continued)

20	Glass	(a)	45	400	4000	84	199	7.90×10^{-3}	0.88	Annealing in Ar for 15 minutes.
		(b)	45	400	4400	80	123	5.40×10^{-3}	0.87	
21	Glass		30	400	2100	84	269	5.64×10^{-3}	0.65	Annealing in Ar for 15 minutes.
22	(a)Glass		45	400	4400	80	70	3.10×10^{-3}	1.53	Annealing in Ar for 15 minutes.
	(b)Fused silica		45	400	4500	90	63	2.83×10^{-3}	5.53	Annealing in Ar for 15 minutes.
23	Glass		90	400	9000	84	69	6.20×10^{-3}	2.53	Annealing in Ar for 25 minutes.

Deposition 2, 3, 4 were done at inlet gas pressure of 9 psi, 10 and 11, at 10 psi and 12.5 at 12 psi, above the atmospheric pressure.

Table 4.2

Calculated X-ray reflections for SnO_2 films.

Iron K_{α_1}, $\lambda = 1.93597$ Å.

Sl. No.	2 θ(°)	θ (°)	d_{hkl}(Å)	$h^2+K^2+2.2L^2=(\frac{a_o}{d_{hkl}})^2$	hkl
1	33.50	16.75	3,358	1.99	(110)
2	42.90	21.45	2,647	3.20	(101),(011)
3	48.10	24.05	2.375	3.98	(200),(020)
4	66.40	33.20	1.768	7.19	(211),(121)
5	70.40	35.20	1.679	7.96	(220)
6	80.20	40.10	1.502	9.95	(310),(130)
7	86.20	43.10	1.416	11.11	(301)

Table 4.3

Standard diffraction data on SnO_2 ·· Radiation: FeK_α; λ = 1.9373 Å.

d_{hkl} (Å)	I/I_1	hkl
3.33	80	110
2.60	80	101
2.36	20	200
2.28	10	111
1.75	100	211
1.67	20	220
1.56	20	002
1.49	20	310
1.42	40	112
1.30	20	202
1.21	20	321
1.18	10	400
1.14	30	222
1.11	10	330
1.082	40	312
1.076	40	411
1.060	20	420
1.020	20	103

Table 4.4

ansmission electron microscopic diffraction data.

terial	Ring No.	Radius 'R' in mm	d_{hkl} (Å)	Camera constant $\lambda L = R d_{hkl}$ (Å.mm.)	Average λL (Å. mm.)
	1	2.25	2.36	5.31	
	2	2.60	2.01	5.30	
.d	3	-	-	-	5.30
	4	4.30	1.23	5.29	

osi- on ıber	Thick- ness (Å)	Material	Ring No.	Radius 'R' in mm	Camera constant λL (Å.mm.)	$d_{hkl} = \frac{\lambda L}{R}$ (Å)
			1	1.575	5.30	3.365
		SnO_2	2	2.000	5.30	2.650
	3700	deposited	3	2.240	5.30	2.366
		on glass	4	3.000	5.30	1.767

5. CONCLUSION

Tin oxide films with satisfactory optical transparencies and sheet resistivities have been prepared. However the solar cell fabricated by depositing these films exhibited poor performance with conversion efficiency of the order of 0.10 percent. The minimum sheet resistivity of 45 Ohms per square for films deposited on glass has been obtained with a considerable loss in optical transmission. For a good solar cell performance sheet resistivities of the order of 5-10 Ohms per square are preferred. Such sheet resistivities should be obtained with possibly no damage to optical transmission.

Improvements in the properties of the film needed for an efficient cell performance could not be obtained owing to some experimental limitations. The first limitation arose from the furnace tube. The tube made of pyrex glass could not withstand the thermal stresses released, when cold solution was sprayed onto the hot zone. Hence after a few depositions the tube developed a severe crack and collapsed. In addition to this, the tube itself acted as a source of contamination by infusing alkali ions into the deposited film and thereby increasing its sheet resistivity. Moreover the maximum temperature that was employed to prevent any possible damage to the tube was around 400 ^{o}C. Both these limitations can to a certain extent be overcome by using fused silica tube.

Thinner films with good electrical conductivity are preferred, because their optical transparencies are quite high.

Such films can be obtained by using some external agents as dopants. Two such reported dopants are antimony chloride ($SbCl_3$) and ammonium fluoride (NH_4F). Both antinony and fluorine act as donors by substituting for tin and oxygen respectively. Such dopants can be added in suitable proportions to the spraying tin chloride solution and thinner films with a good conductivity can be deposited as barrier layers on Si.

The deposited films can be subjected to heat treatment at higher temperatures in the range of 500-600 ^{o}C, as at temperatures in between 240 and 380 ^{o}C are found processes which oxidise metallic tin to SnO_2. To secure a good conductivity, metallic tin is preferred to be present in the films. The tin content in the film is increased at high temperatures by the oxidation of SnO to SnO_2 and metallic tin. For the same purpose, some reducing agents such as pyrogallol have also been used to lower the oxidation of metallic tin during the deposition.

A continuous spray is also equally necessary to get films with some reproducibility in their properties. For this, the pressure build-up in the furnace tube rendering the spray discontinuous is to be avoided. To meet these requirements, efficient gas regulator valves, flowmeters and an exhaust, which can sweep out the inlet gas swiftly are essential.

References

1. T. Nagatomo and O. Omoto, "Electrical and Optical properties of indium oxide/n-Si photodiodes", Jap. J. App. Phys. 15, 199 (1976).

2. I. Mizrah and D. Adler, "Operation of ITO/n-Si heterojunction solar cells", App. Phys. Lett., 29, 682 (1976).

3. K. Kajiyama and Y. Furukawa, "Electrical and Optical properties of SnO_2/Si heterojunctions", Jap. J. App. Phys. 6, 905 (1967).

4. H. Kato, A. Yoshida and T. Arizumi, "A simple fabrication method of SnO_2/Si solar cell", ibid, 15, 1819 (1976).

5. J.C.C. Fan and F.J. Bachner, "Thin film conducting microgrids as transparent heat mirrors", App. Phys. Lett., 28, 440 (1976).

6. R.R. Mehta and S.F. Vogel, "Sputtered cadmium oxide and indium oxide/tin oxide as transparent electrodes to cadmium sulphide", J. Electrochem. Soc. 119, 752 (1972).

7. J.C.C. Fan and F.J. Bachner, "Properties of Sn doped In_2O_3 films prepared by R.F. sputtering", J. Electrochem. Soc. 122, 1719 (1975).

8. G. Haacke. "Transparent conducting coatings", Ann. Rev. Mat. Sc. 7, 73 (1977).

9. N.S. Chang and J.R. Sites, "Electronic characterisation of ITO/Si photodiode", J. App. Phys. 49, 4833 (1978).

10. J.B. Dubow, D.E. Burk, J.R. Sites, "Efficient photovoltaic heterojunctions of indium tin oxides on silicon", App. Phys. Lett. 29, 494 (1976).

11. Z.M. Jarzebski, ''Oxide semiconductors'', Pergamon Press, New York, 1973.

12. T. Nishino and Y. Hamakawa, "Electrical and Optical properties of Si-SnO_2 heterojunctions'', Jap. J. App. Phys. 9, 1085 (1970).

13. Sihvonen Y.T., Boyel D.R., ''Transparent indium contacts to cadmium sulphide'', Rev. Sci. Instr. 31, 992 (1960)

14. J.C.C. Fan, ''Preparation of Sn doped In_2O_3 (ITO) at low deposition temperatures by ion beam sputtering'', App. Phys. Lett. 34, 515 (1979).

15. T. Muranoi and M. Furukoshi, ''Properties of stannic oxide thin films produced from $SnCl_4$-H_2O and $SnCl_4$-H_2O_2 reaction systems'', Thin solid films, 48, 309 (1978).

16. Köstlin H., Jost R., Lems W., ''Optical and electrical properties of doped indium oxide films'', Phy. Stat. Sol., 29, 87 (1975).

17. Tom Feng, Amal K. Ghosh, Charles Fishman, ''Spray deposited high efficiency SnO_2/n-Si solar cells'', App. Phys. Lett. 35, 266 (1979).

18. S. Kulaszewicz, I. Lasoka, and CZ. Michalski, " Properties of transparent conducting films of SnO_2:Sb and In_2O_3:Sn deposited by hydrolysis'', Thin Solid Films 55, 283 (1978).

19. S. Ashok, P.P. Sharma and S.J. Fonash, '' Spray deposited ITO/Si heterojunction solar cells'', a report from Pennsylvania State University.

20. K.P. SreeHarsha, K.J. Bachman, P.H. Smidt, E.G. Spencer and F.A. Thiel, "n-indium tin oxide/p-indium phoside solar cells", App. Phys. Lett. 30, 645 (1977).

21. A.L. Fahrenbruch, J. Aranovich, F. Courreges, T. Chynoweth, and P.H. Bube, "Recent investigation of metal oxide/silicon heterojunction solar cells", Thirteenth IEEE photovoltaic specialist's conference, p 281, 1978.

22. T. Arizumi, A. Yoshida, H. Kato, and S. Morinaga, "Photosensitive Si-SnO_2 heterojunction diodes", Iranian. J. Science and Technology, 4, 95 (1976).

23. E.Y. Wang and R.N. Legee, "General properties of SnO_2-GaAs and SnO_2-Ge heterojunction photovoltaic cells", IEEE Trans. Electron devices, ED-25, 800 (1978).

24. Maissel and Glang, "Hand book of Thin Film Technology", McGraw Hill Book Co., New York.

25. S. Samson and C.G. Fonstad, "Defect structure and electronic donor levels in SnO_2 crystals", J. App. Phys. 44, 4618 (1973).

26. M. Nagasawa and S. Shinoyo, "Electrical and optical properties of reduced stannic oxide crystals", Jap. J. Appl. Phys. 10, 472 (1971).

27. M. Nagasawa and S. Shinoyo, " Weak field magnetoresistance in SnO_2 single crystals", J. Phys. Chem. Sol. 29, 1959 (1968).

28. J.A. Marley and R.C. Dockerty, "Electrical properties of stannic oxide single crystals", Phys. Rev. 140A, 304 (1965).

29. J.A. Aboalf, J.C. Marcotte and N.J. Chou, "Chemical composition and electrical properties of tin oxide films prepared by vapor deposition", J. Electrochem. Soc. 120, 701 (1973).

30. G. Haacke, "New figure of merit for transparent conductors", J. App. Phys. 47, 4086 (1976).

31. T. Arai, "The study of optical properties of conducting tin oxide films and their interpretation in terms of a tentative band scheme", J. Phys. Soc. Japan, 15, 916 (1960).

32. "International center for X-ray diffraction data" (JCPDS), 1978.

33. A.K. Ghosh, C. Fishman, and T. Feng, "SnO_2/Si solar cell - heterostructure or Schottky barrier or MIS type device", J. App. Phys. 49, 3490 (1978).

34. R.L. Anderson, "Photocurrent suppression in heterojunction solar cells", App. Phys. Lett. 27, 691 (1975).

35. S.J. Fonash, "The role of the interfacial layer in metal semiconductor solar cells", J. App. Phys. 46, 1286 (1975).

36. J. Shewchun, R. Singh and M.A. Green, "Theory of metal insulator-semiconductor solar cell", ibid, 48, 765 (1977).

37. H.C. Card and E.S. Yang, "MIS Schottky theory under conditions of optical carrier generation in solar cells", App. Phys. Lett. 29 51 (1976).

38. S. Kar, S. Ashok and S.J. Fonash, "Evidence of tunnel assisted transport in nondegenerate MOS and Semiconductor-oxide-Semiconductor diodes at room temperature", J. App. Phys. 51, 3417 (1980).

39. S. Kar, ''On the role of interface states in MOS solar cells'', J. App. Phys. 49 5278 (1978).

Figure Captions

Fig. 2.1 Equivalent circuit diagram of a solar cell. I_D is the diode current, R the series resistance, and R_L the load resistance.

Fig. 2.2 Energy band diagram of SnO_2/SiO_x/n-Si solar cell in equilibrium.

Fig. 3.1a Diagram of spraying unit.

Fig. 3.1b Sprayer unit, furnace tube, exhaust unit assembly.

Fig. 3.2 Block diagram indicating the sequence of steps followed for fabrication of SnO_2/SiO_x/n-Si solar cells.

Fig. 3.3 Side view and top view of SnO_2/SiO_x/n-Si solar cell showing front metal grid contact and back ohmic contact.

Fig. 3.4a Circuit diagram of the set-up used for measuring current-voltage characteristics of solar cells.

Fig. 3.4b Circuit diagram of the set-up used for the measurement of diode current-voltage characteristics.

Fig. 3.4c Circuit diagram of the set-up used for measuring the capacitance-voltage characteristics of solar cells.

Fig. 4.1 Transmittance of films plotted as a function of their sheet resistivity.

Fig. 4.2 Transmittance and absorbance of the film on fused silica plotted as a function of wavelength.

Fig. 4.3 Transmittance plotted as a function of wavelength for comparing the transmittance characteristics of film on glass with that on fused silica.

Fig. 4.4 Transmittance, reflectance and absorptance of film on glass plotted as a function of wavelength.

Fig. 4.5 Transmittance of films on glass, plotted as a function of wavelength to show the variation of transmittance characteristics with sheet resistivity and film thickness.

Fig. 4.6 Square root of absorption coefficient of a film on fused silica plotted as a function of photon energy for evaluating the band gap of tin oxide.

Fig. 4.7a X-ray diffractogram of tin oxide film obtained by using iron K_α radiation.

Fig. 4.7b Transmission electron diffraction pattern of tin oxide film.

Fig. 4.8 Transmission electron micrograph of tin oxide film of sheet resistivity 4500 Ohms per square.

Fig. 4.9 Transmission electron micrograph of tin oxide film of sheet resistivity 123 Ohms per square.

Fig. 4.10 Current-voltage characteristics of $SnO_2/SiO_x/n\text{-}Si$ solar cell.

Fig. 4.11 Linear plot of diode current-voltage characteristics.

Fig. 4.12 Semilogarthmic plot of diode current-voltage characteristics.

Fig. 4.13 Reciprocal of squared capacitance plotted as a function of applied bias.

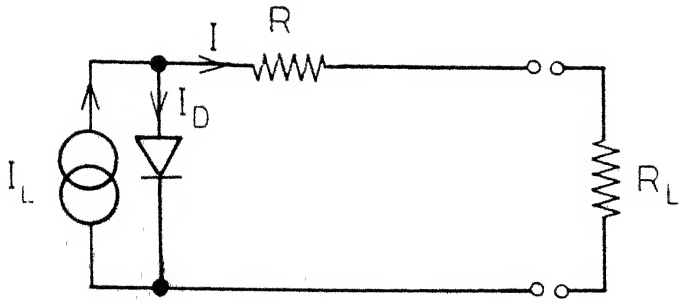
I
R
I_D
I_L
R_L

Fig 2 1

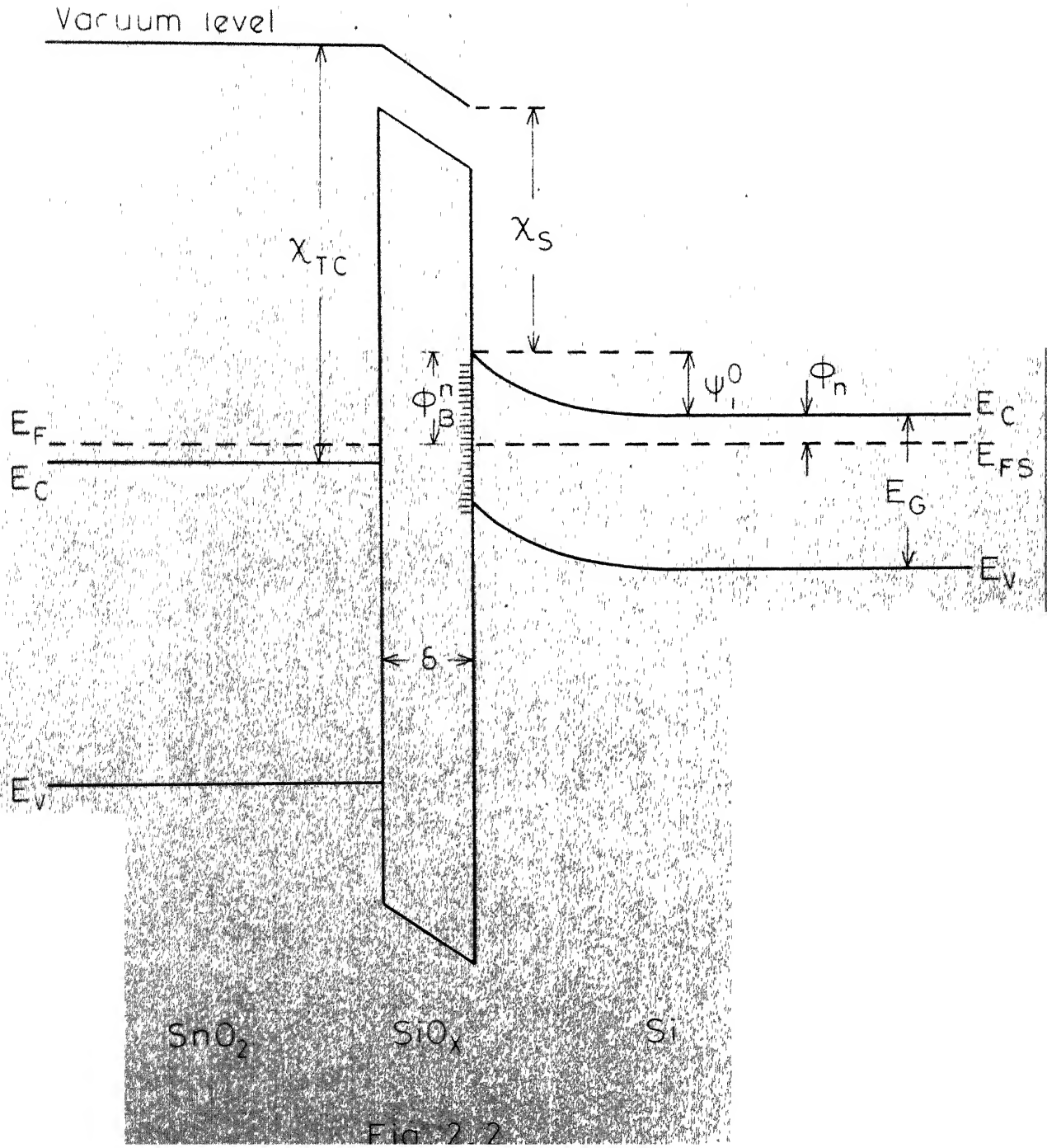
Vacuum level
χ_{TC}
χ_S
Φ_B^n
ψ_i^0
Φ_n
E_F
E_C
E_{FS}
E_G
E_V
δ
SnO_2
SiO_x
Si

Fig 2 2

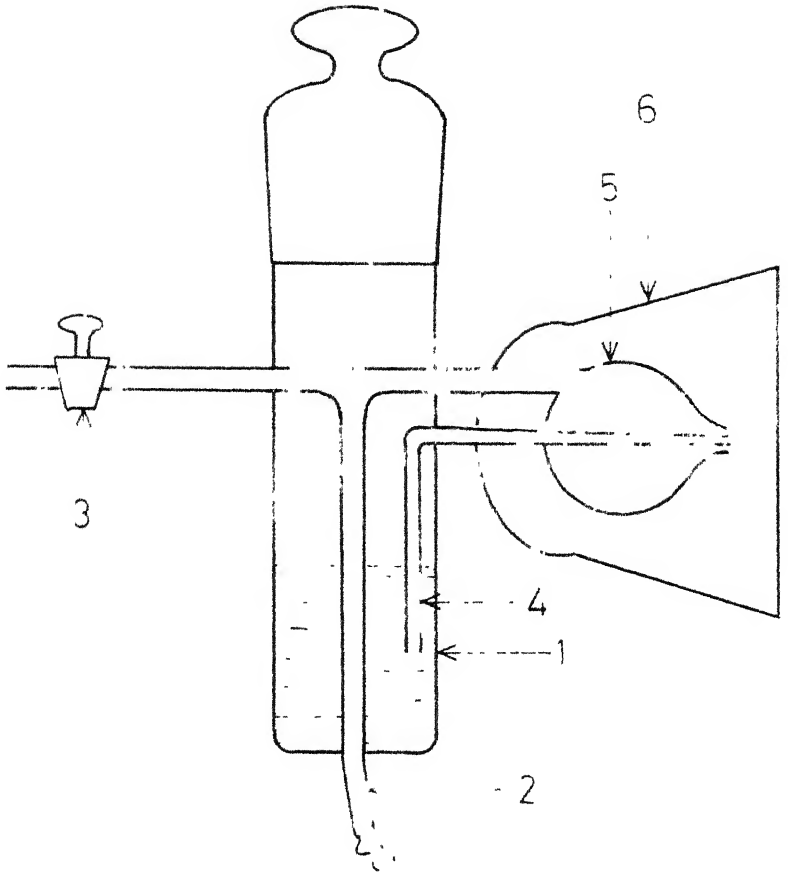

1 Reservoir
2 Gas inlet tube
3 Stop cock to initiate spraying
4 Suction tube
5 Gas expansion bulb
6 Ground glass socket

Fig 3.1a

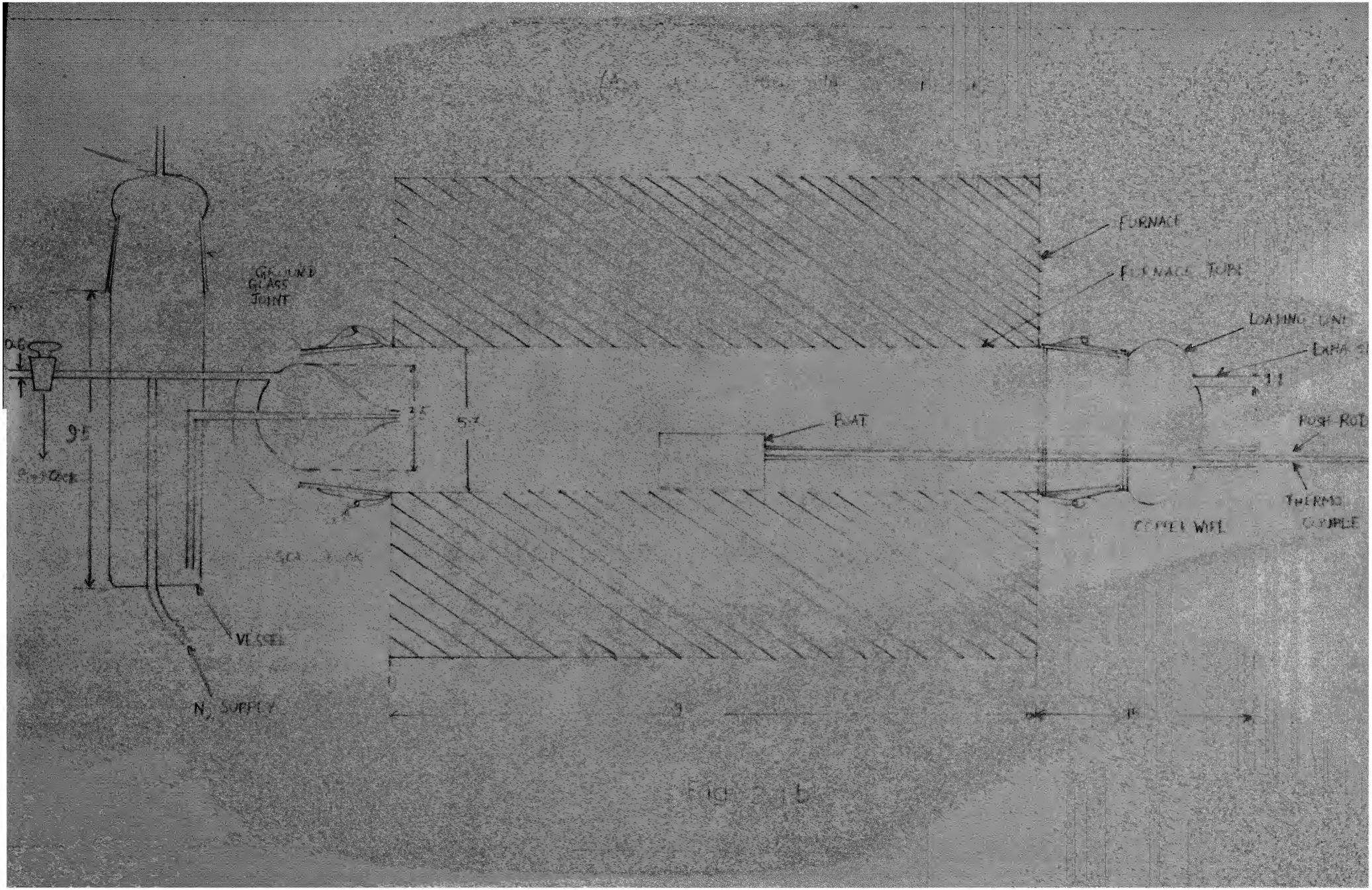
GROUND GLASS JOINT
0.6
9.5
3.5
5.7
VESSEL
N2 SUPPLY
FURNACE
FURNACE TUBE
LOADING LINE
EXPA
11
FLAT
PUSH ROD
THERMO COUPLE
COPPER WIRE
9
15

FIG 2.1b

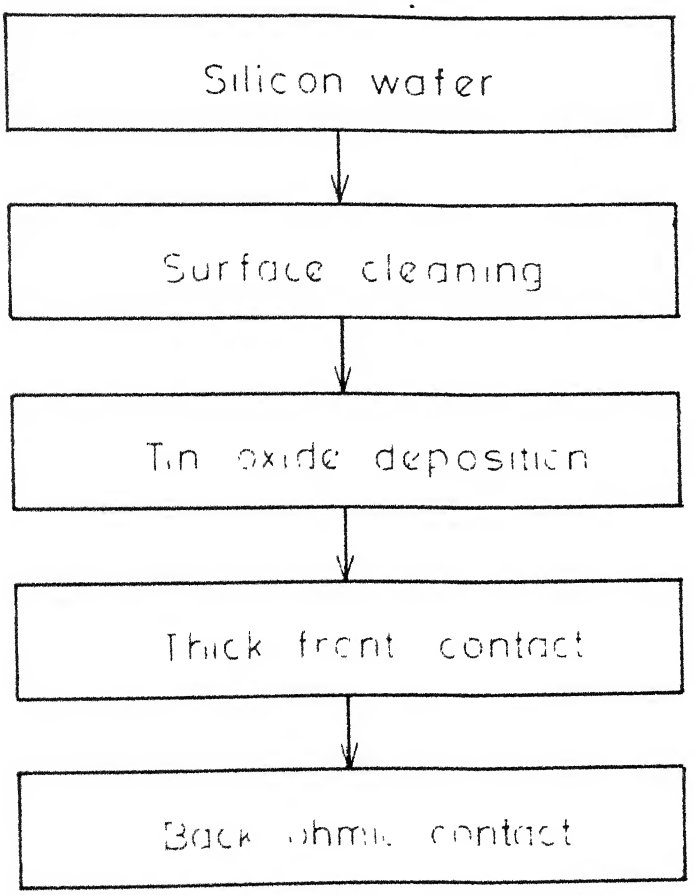
Silicon wafer
Surface cleaning
Tin oxide deposition
Thick front contact
Back ohmic contact

Fig 3.2

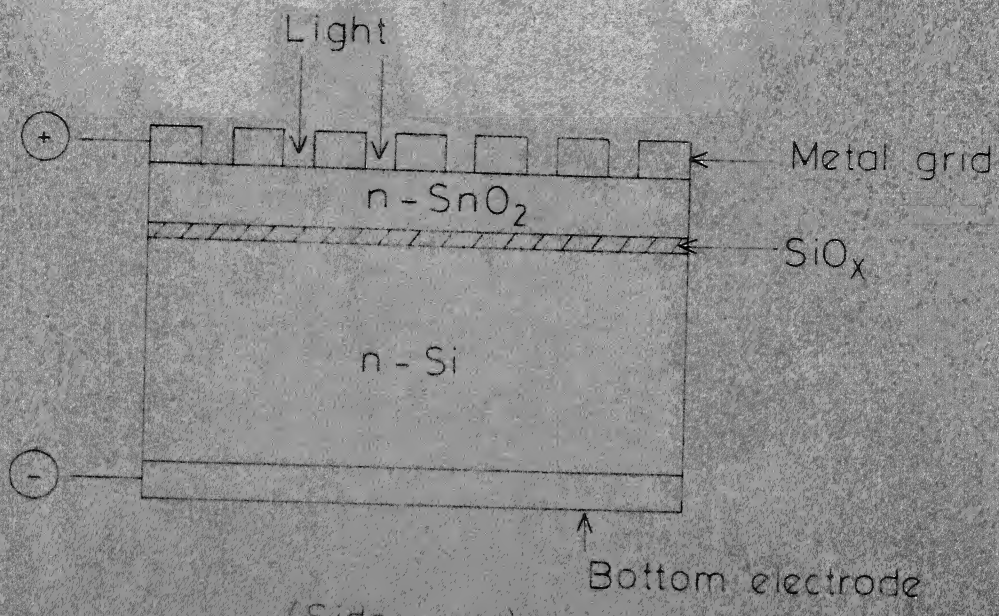

(Side view)

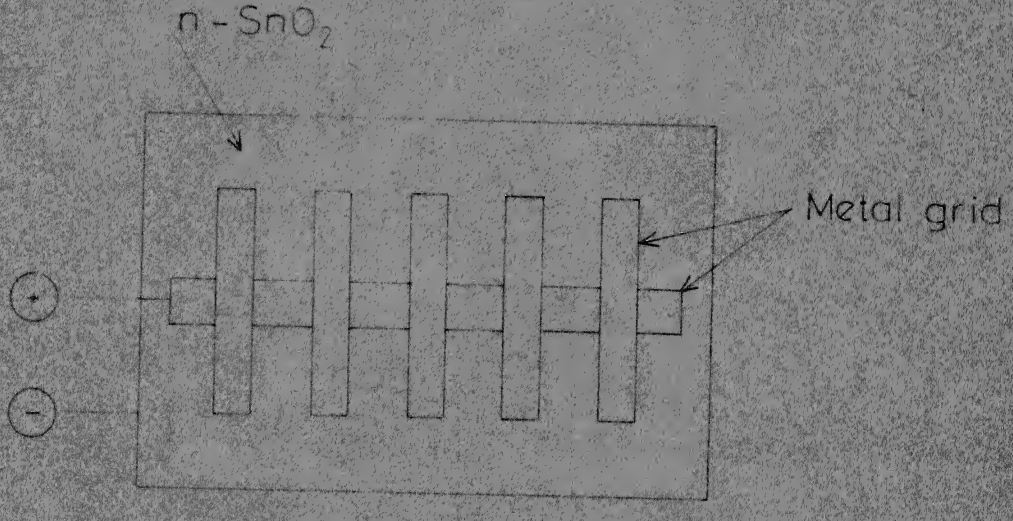

(Top view)

Fig. 3.3

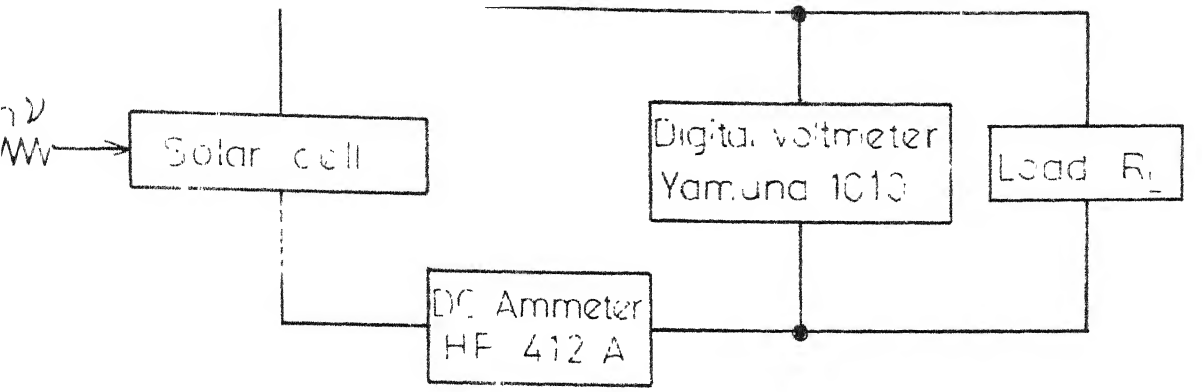

Fig 3.4a

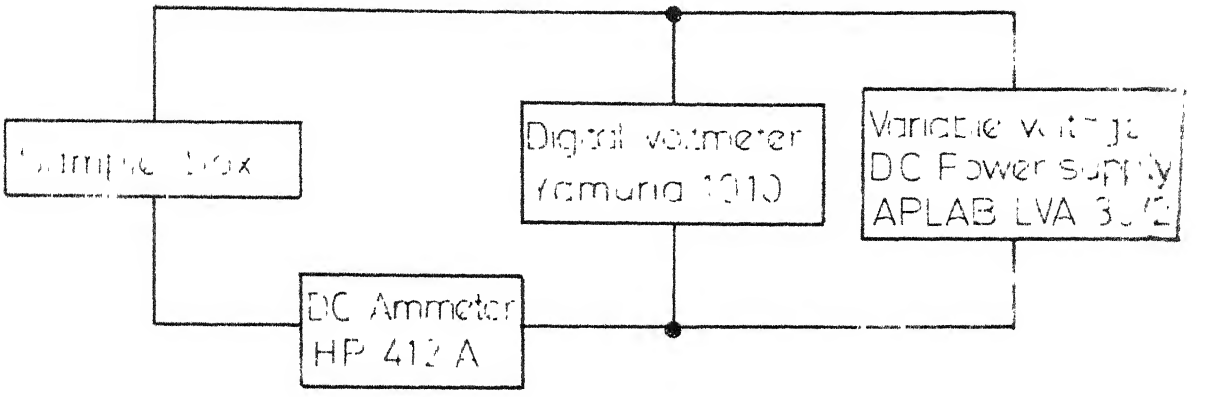

Fig 3.4b

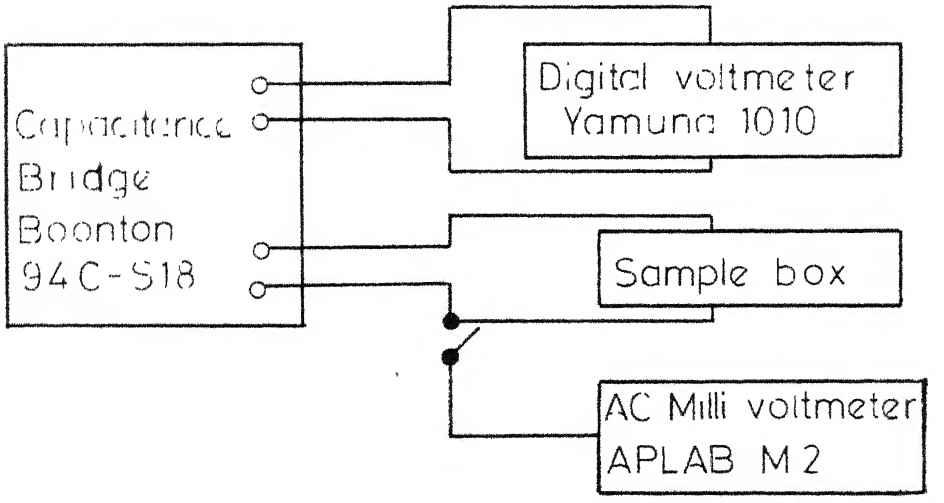

Fig. 3.4c

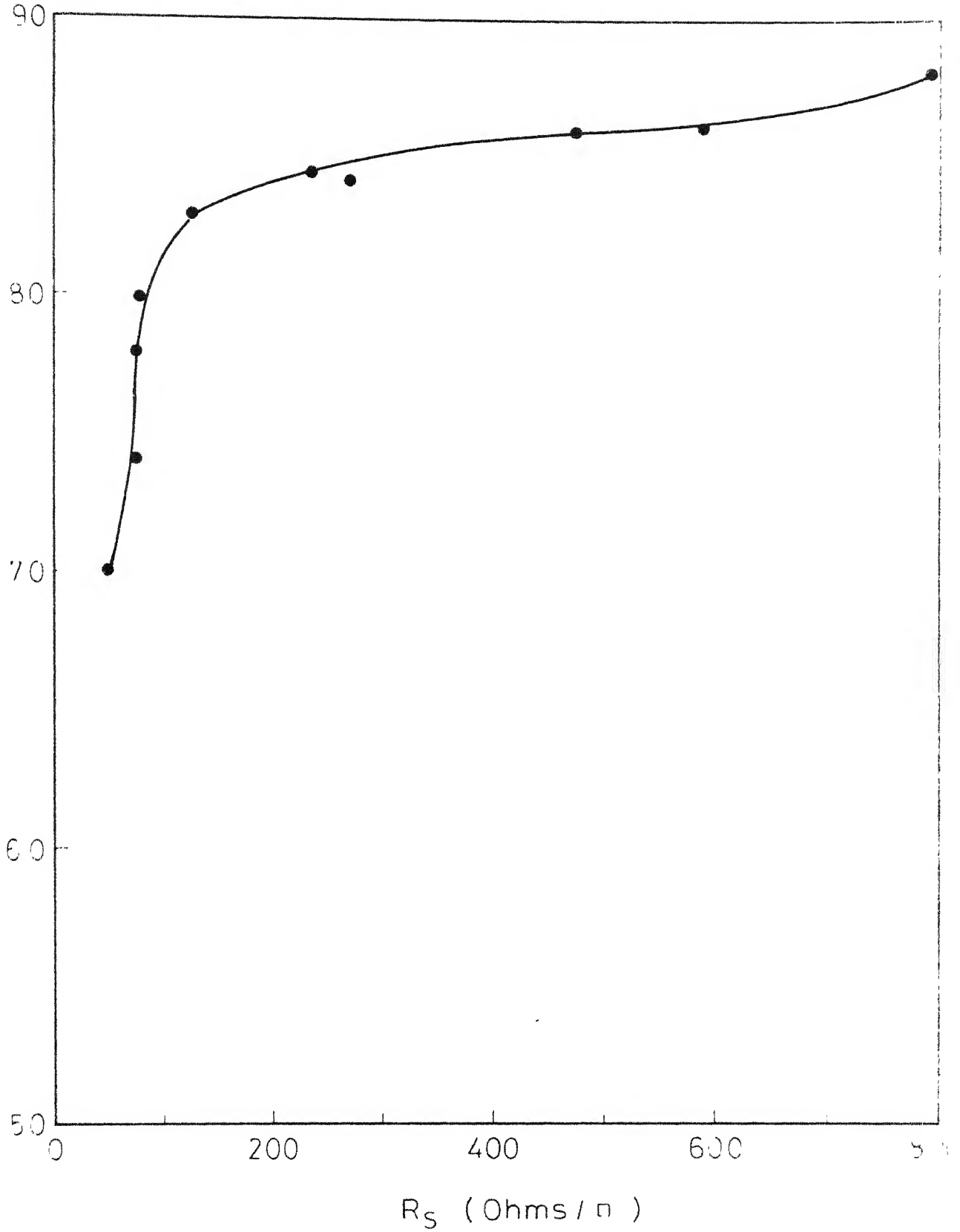

Fig. 4 1

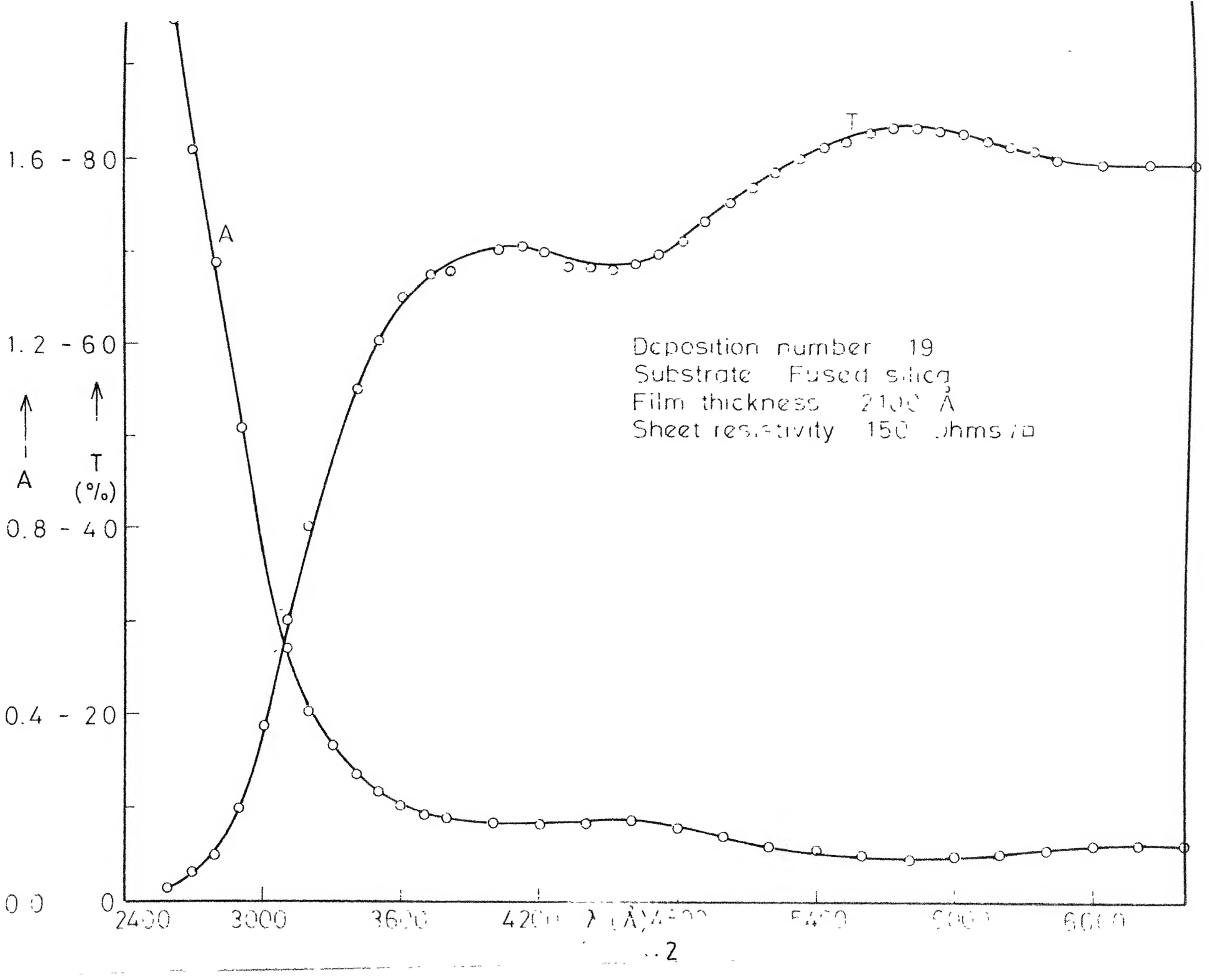
1.6 - 80
1.2 - 60
0.8 - 40
0.4 - 20
0 0
A
T
(%)
0
2400
3000
3600
T
A
Deposition number 19
Substrate Fused silica
Film thickness 2100 Å
Sheet resistivity 150 ohms/□

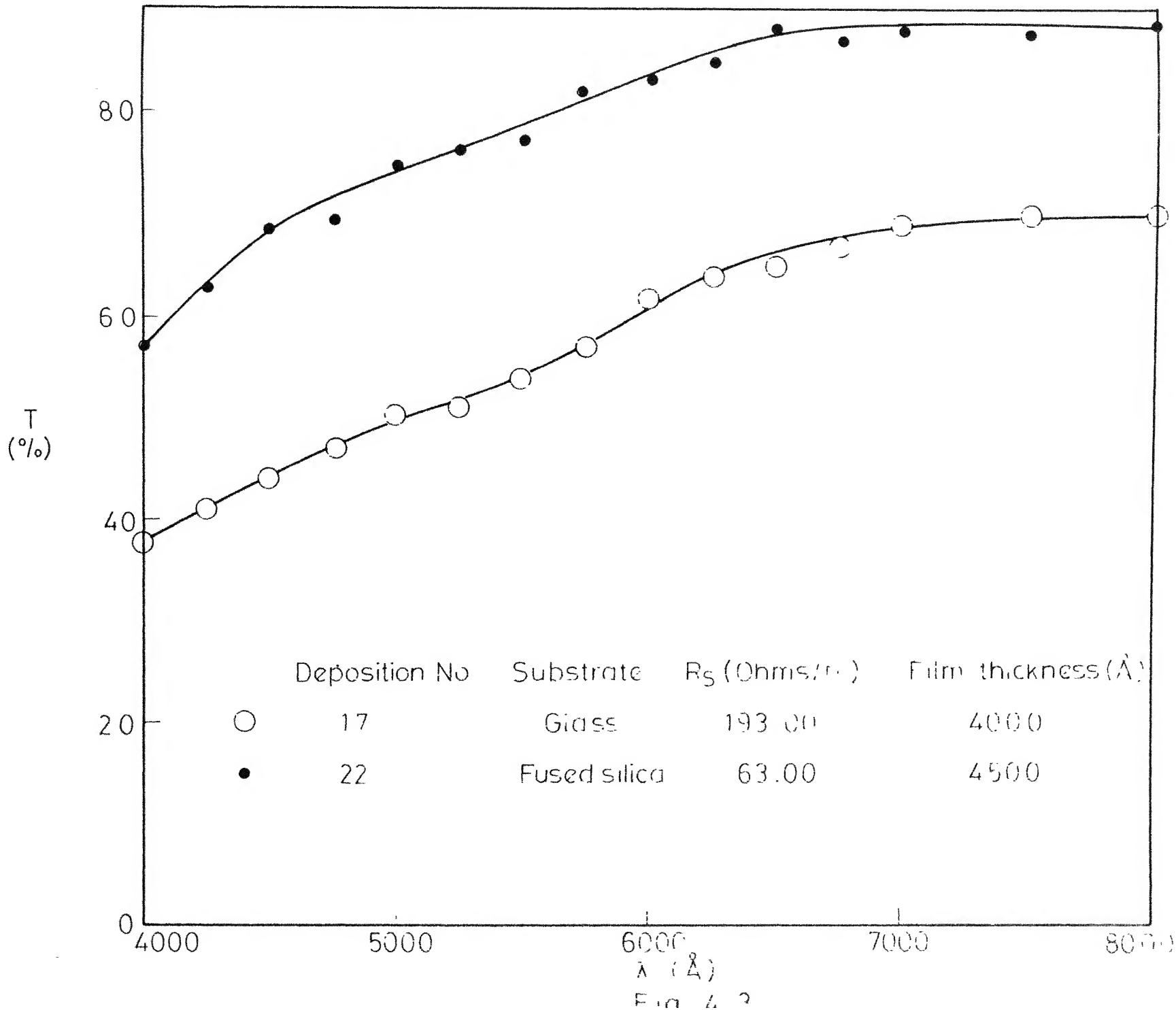
80
60
40
20
0
T
(%)
4000
5000
6000
7000
λ (Å)
Deposition No
Substrate
Rs (Ohms/□)
Film thickness (Å)
17
Glass
4000
22
Fused silica
63.00
4500

Fig. 4.3

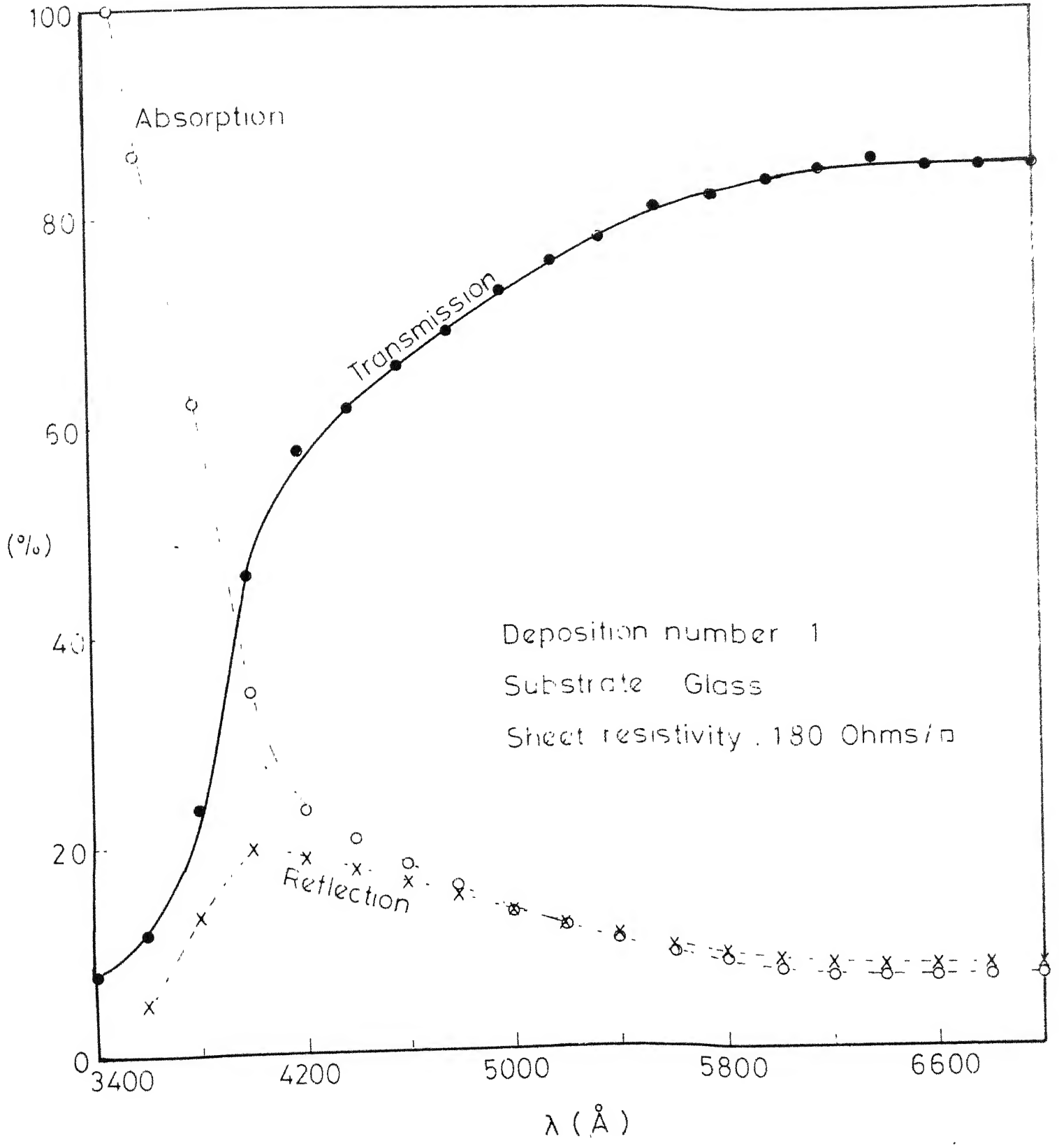
100
80
60
40
20
0
(%)
Absorption
Transmission
Reflection
Deposition number 1
Substrate Glass
Sheet resistivity . 180 Ohms/□
3400
4200
5000
5800
6600
λ (Å)

Fig. 4 4

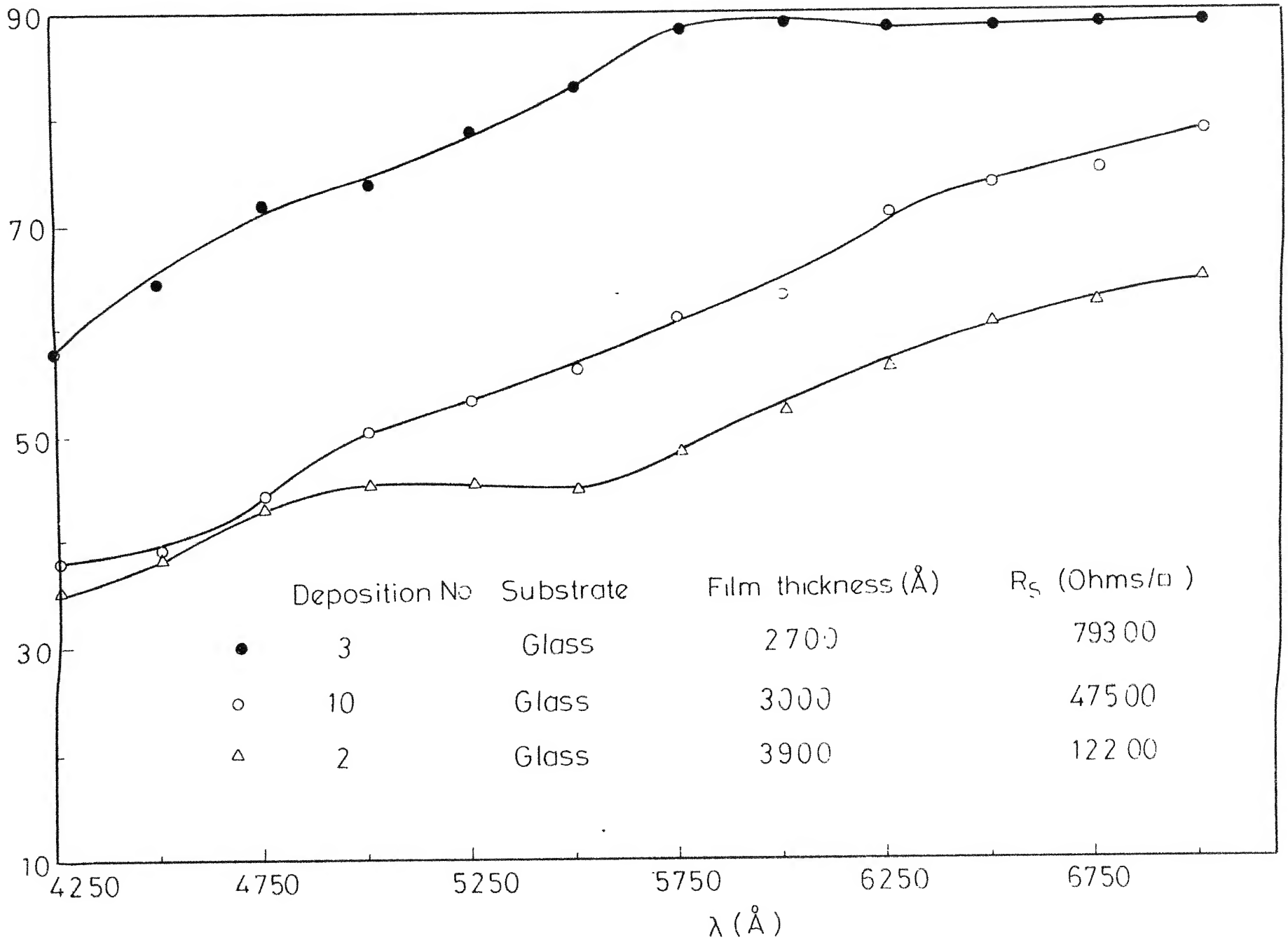
90
70
50
30
10
T
(%)
4250
4750
5250
5750
6250
6750
λ (Å)
Deposition No
Substrate
Film thickness (Å)
Rs (Ohms/□)
3
Glass
2700
79300
10
Glass
3000
47500
2
Glass
3900
12200

Fig 4.5

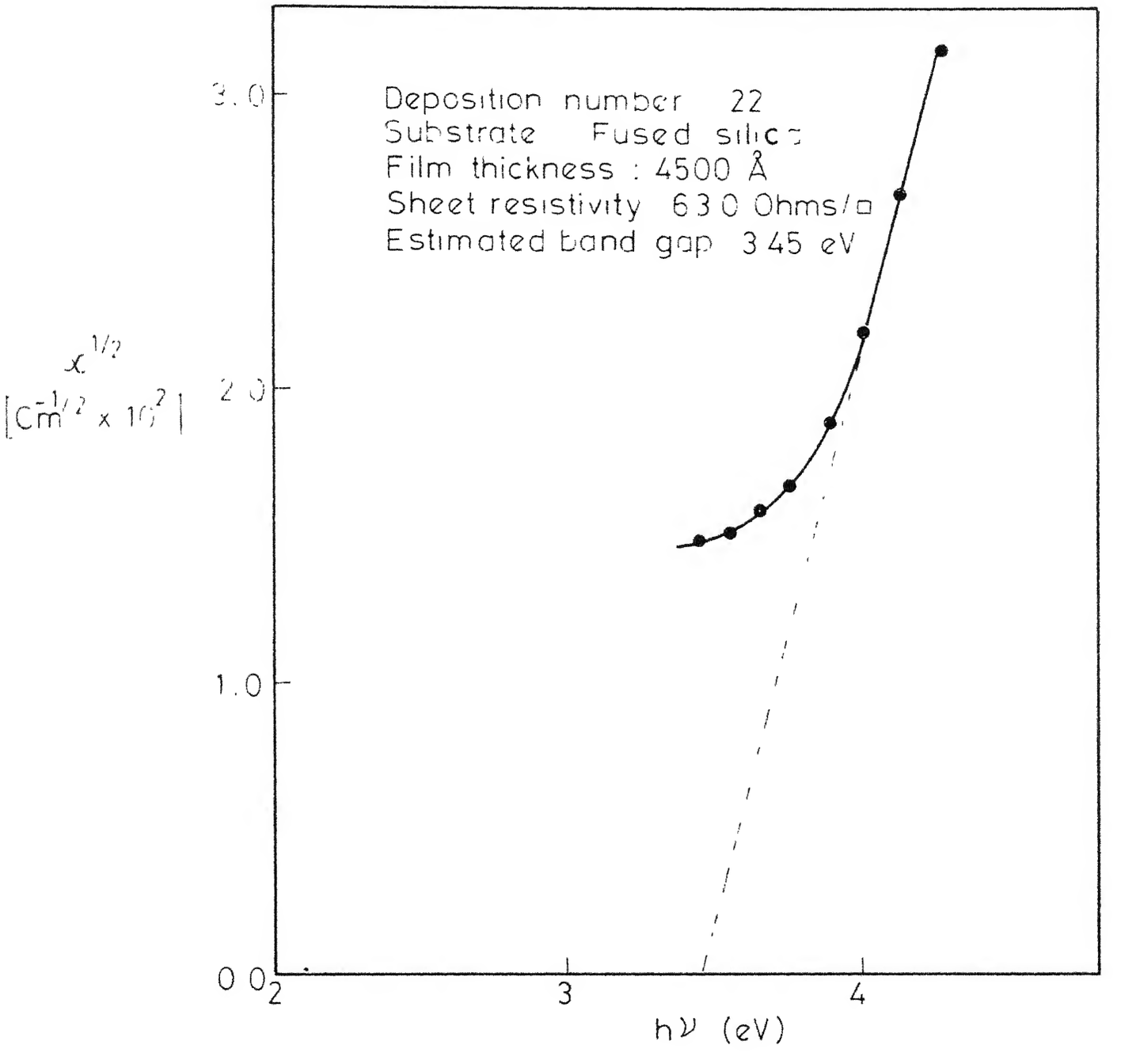
Deposition number 22
Substrate Fused silica
Film thickness : 4500 Å
Sheet resistivity 630 Ohms/□
Estimated band gap 3.45 eV
$\alpha^{1/2}$
$[Cm^{-1/2} \times 10^2]$
3.0
2.0
1.0
0.0
2
3
4
hν (eV)

Fig. 4 6

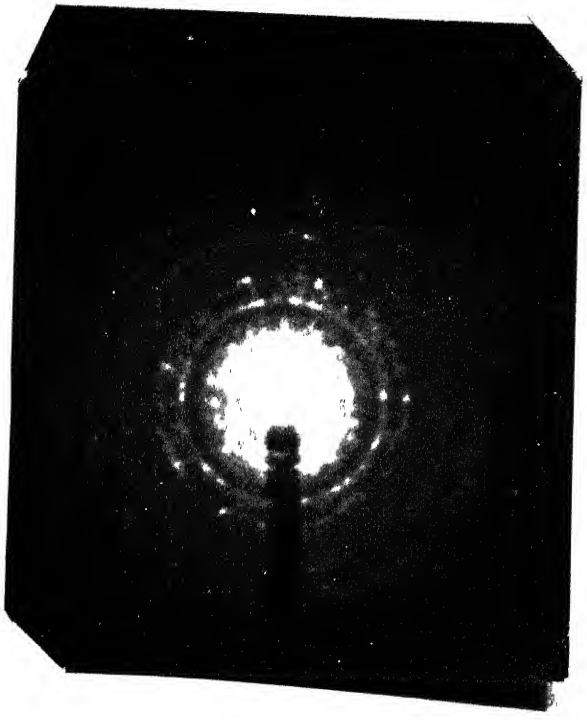

Fig. 4.7b

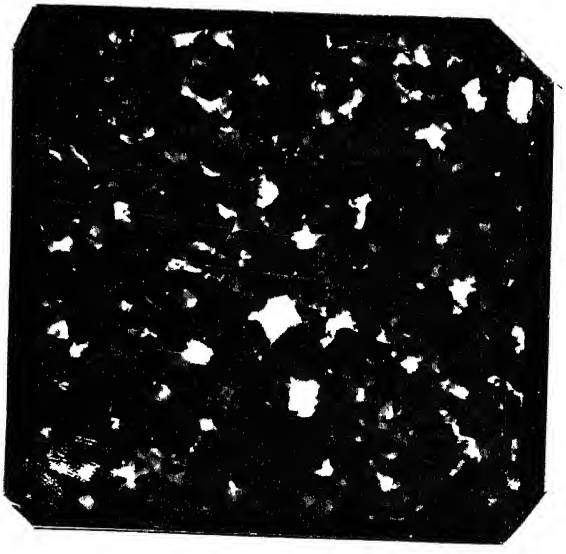

Fig. 4.8

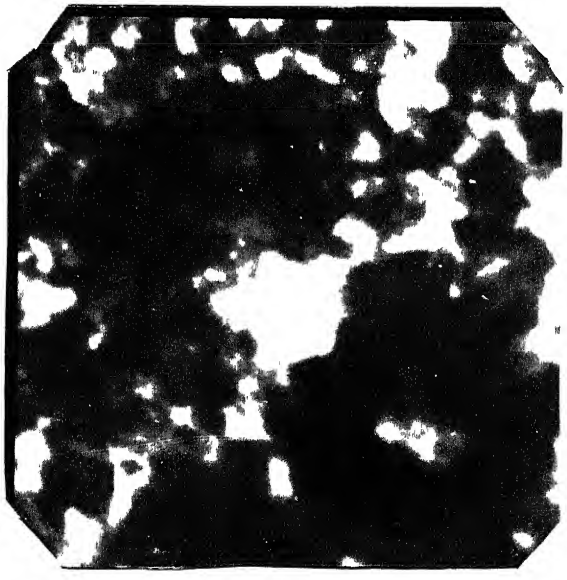

Fig. 4.9

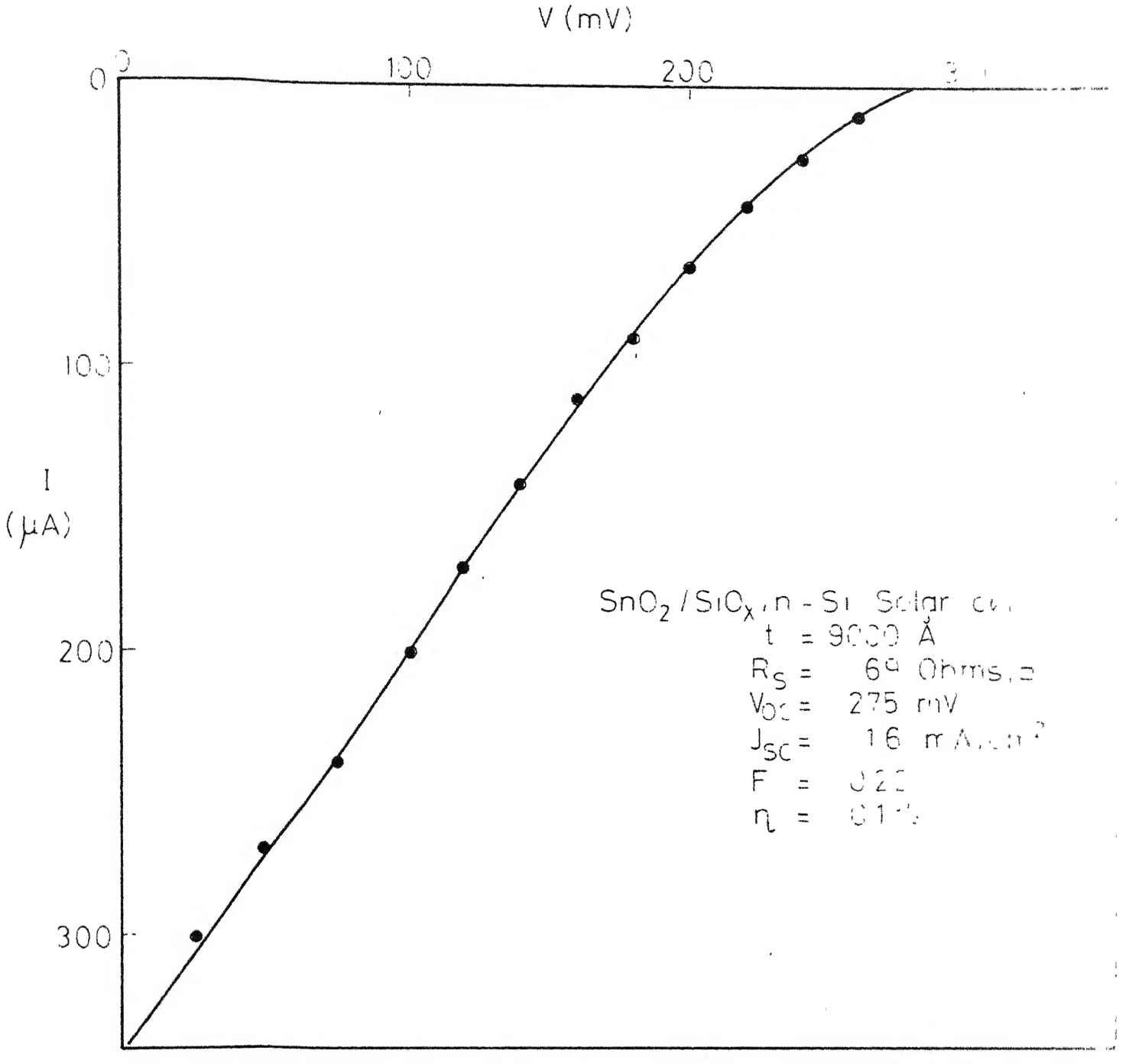
V (mV)
0
100
200
100
200
300
I
(μA)
SnO_2 / SiO_x / n - Si Solar cell
t = 9000 Å
R_S = 69 Ohms.cm
V_{OC} = 275 mV
J_{SC} = 16 mA/cm²
F = 0.22
η = 0.1%

Fig 410

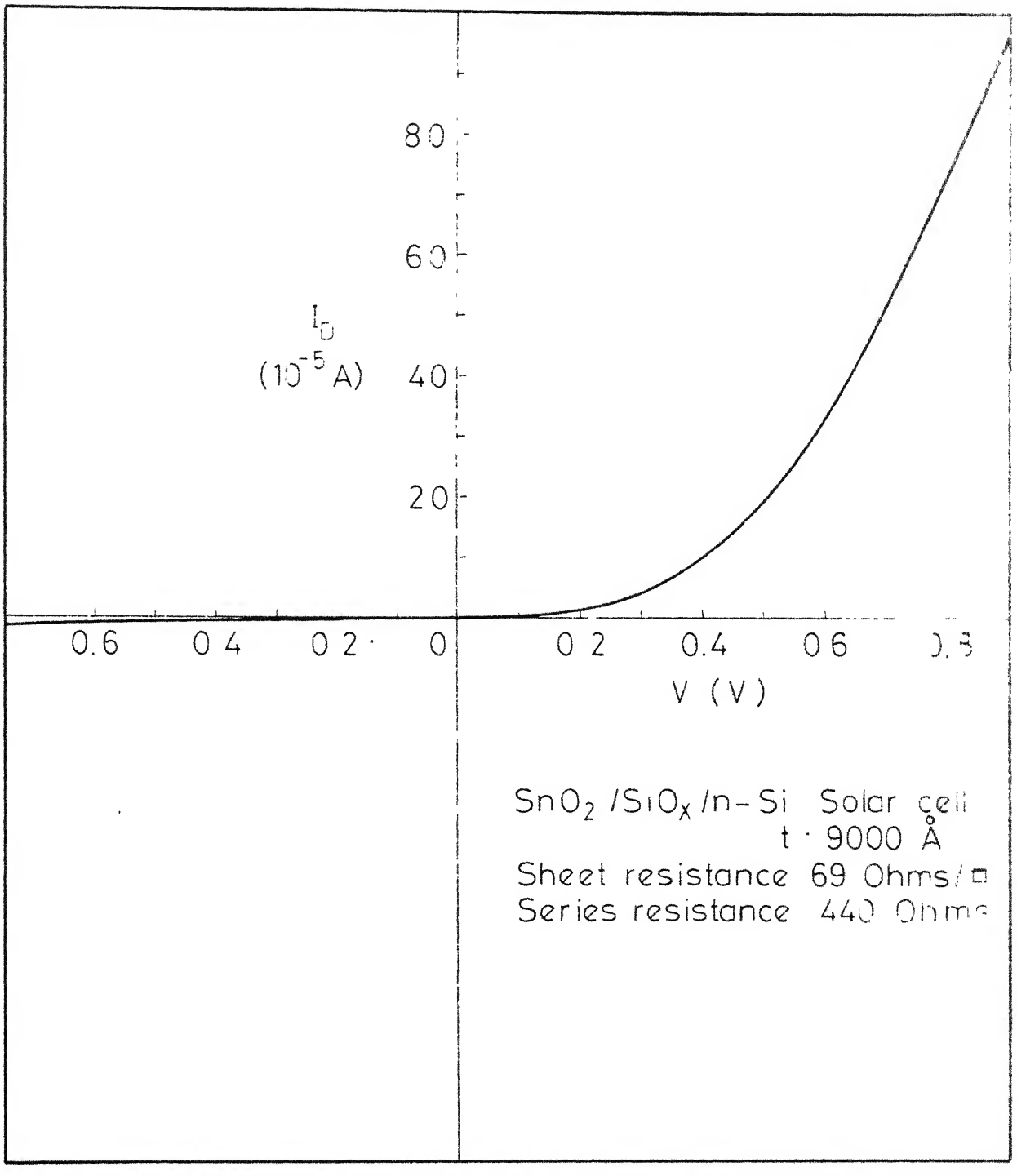
80
60
40
20
I_D
$(10^{-5}$ A)
0.6
0 4
0 2
0
0 2
0.4
0 6
V (V)
SnO_2 /SiO_x /n-Si Solar cell
t · 9000 Å
Sheet resistance 69 Ohms/□
Series resistance 440 Ohms

Fig. 4.11

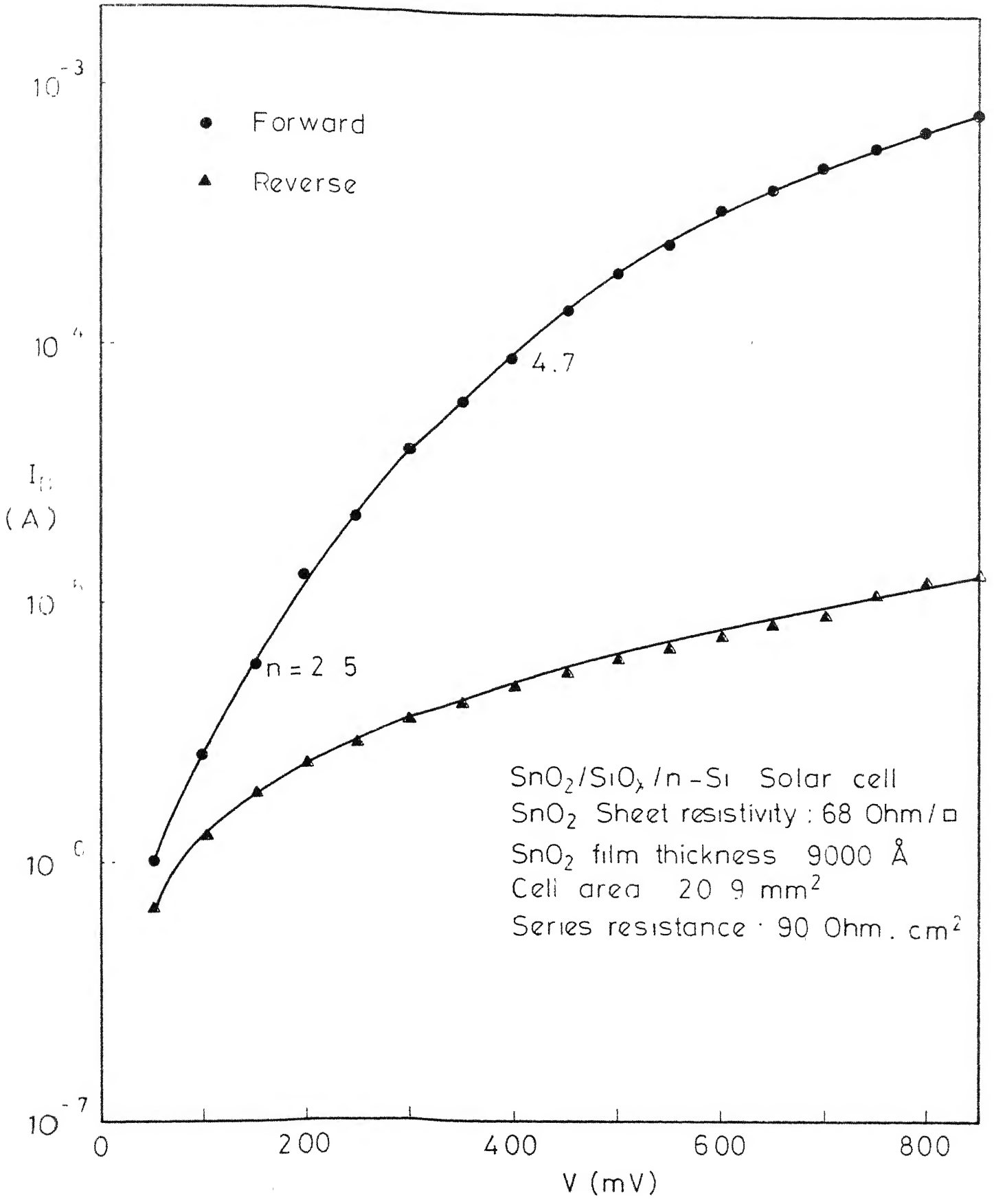
Forward
Reverse
4.7
n = 2 5
$SnO_2/SiO_x/n-Si$ Solar cell
SnO_2 Sheet resistivity : 68 Ohm/□
SnO_2 film thickness 9000 Å
Cell area 20 9 mm^2
Series resistance · 90 Ohm . cm^2
10^{-3}
10^{-4}
10^{-5}
10^{-6}
10^{-7}
I_F
(A)
0
200
400
600
800
V (mV)

Fig. 4.12

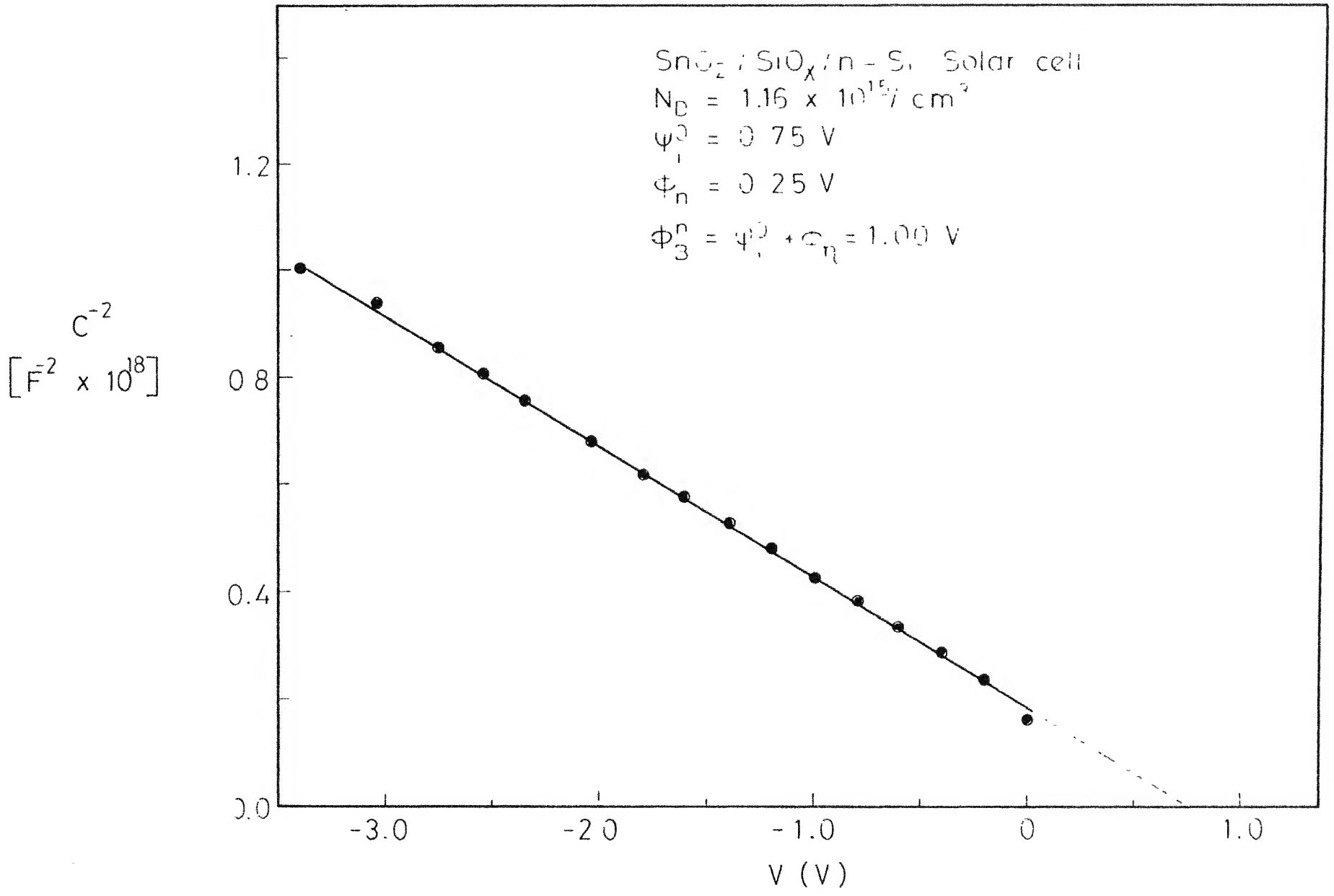
SnO_2 / SiO_x / n - Si Solar cell
N_D = 1.16 x 10^{15} / cm^3
ψ_i^n = 0.75 V
Φ_n = 0.25 V
$\Phi_3^n = \psi_i^n + \Phi_n$ = 1.00 V
C^{-2}
$[F^{-2} \times 10^{18}]$
1.2
0.8
0.4
0.0
-3.0
-2.0
-1.0
0
1.0
V (V)

Fig. 4.13